University of Alberta

Modeling transport of thermalized neutrals in a sputter deposition system

by

Francisco J. Jimenez

A thesis submitted to the Faculty of Graduate Studies and Research in partial fulfillment of the requirements for the degree of **Master of Science**.

Department of Electrical Engineering

Edmonton, Alberta
Spring 2005

0-494-08091-4

Library and Archives Canada

Published Heritage Branch

395 Wellington Street
Ottawa ON K1A 0N4
Canada

Bibliothèque et Archives Canada

Direction du Patrimoine de l'édition

395, rue Wellington
Ottawa ON K1A 0N4
Canada

Your file *Votre référence*
ISBN:
Our file *Notre reference*
ISBN:

NOTICE:
The author has granted a non-exclusive license allowing Library and Archives Canada to reproduce, publish, archive, preserve, conserve, communicate to the public by telecommunication or on the Internet, loan, distribute and sell theses worldwide, for commercial or non-commercial purposes, in microform, paper, electronic and/or any other formats.

The author retains copyright ownership and moral rights in this thesis. Neither the thesis nor substantial extracts from it may be printed or otherwise reproduced without the author's permission.

AVIS:
L'auteur a accordé une licence non exclusive permettant à la Bibliothèque et Archives Canada de reproduire, publier, archiver, sauvegarder, conserver, transmettre au public par télécommunication ou par l'Internet, prêter, distribuer et vendre des thèses partout dans le monde, à des fins commerciales ou autres, sur support microforme, papier, électronique et/ou autres formats.

L'auteur conserve la propriété du droit d'auteur et des droits moraux qui protège cette thèse. Ni la thèse ni des extraits substantiels de celle-ci ne doivent être imprimés ou autrement reproduits sans son autorisation.

In compliance with the Canadian Privacy Act some supporting forms may have been removed from this thesis.

While these forms may be included in the document page count, their removal does not represent any loss of content from the thesis.

Conformément à la loi canadienne sur la protection de la vie privée, quelques formulaires secondaires ont été enlevés de cette thèse.

Bien que ces formulaires aient inclus dans la pagination, il n'y aura aucun contenu manquant.

Canada

What makes the desert beautiful is that somewhere it hides a well.

Antoine de Saint-Exupery

To

My parents for their love and support.

Para

Mis padres por su amor y apoyo.

Abstract

Thermalization of energetic neutrals produced at the target in a typical magnetron sputter deposition system occurs as energetic particles collide with background gas atoms. After thermalization, transport of neutrals is believed to be governed by diffusion phenomena. This effect is responsible for reducing the energy of incoming particles to the substrate which in turn affects the quality and characteristics of the film being deposited. A coupled model that approximates transport of the thermalized particles in a typical magnetron sputter chamber is presented. The thermalized model follows a fluid approach to predict steady state spatial distributions of thermalized particles as a function of position. Particle diffusion is coupled with an anergy solver to consider the effect of gas heating on particle and energy flux at the substrate.

Acknowledgements

I wish to express my sincere gratitude to my supervisor Dr. Steve Dew, who guided and financially supported this work. He was always helpful providing guidance throughout my research. He also aided in the proper editing of this document.

I am also grateful to the old and new members of Steve Dew's research group for their support throughout the course of this thesis. I have had the pleasure of collaborating with several people who have been very inspiring: Maria Stepanova and Samuel Ekpe for their support whenever it was needed, Patricia Beatty, likely the only person in the world that knows all the intricate structure of the SPUDII project, for her patience and her explanation of the project, and Dr. Yunfeng Shao for the interesting and helpful discussions. Finally, I would like to thank Dr. David Field for his insight and constant guidance regarding the fascinating topics involving magnetrons, especially plasmas. He is also responsible for the corrections of my English and elimination of the inherent grammatical and structural errors when writing in a second language.

I would like to acknowledge the financial support of CONACYT, Mexico. Without their initial financial support this journey would not have been possible.

Last, but not least, I would like to express my deepest gratitude for the constant friendship and comradery of my friends in Edmonton, especially to those who speak the same language as myself. Without their friendship this would have been a more difficult task to accomplish.

I dedicate this thesis to Javier, Maria Graciela, Miguel, Luis Fernando and Monica, and my family. I would also like to dedicate this work to my uncle Miguel who unfortunately is no longer with us. I have no words to express my affection towards them.

Contents

1 Introduction **1**
- 1.1 Thin films . . . 1
- 1.2 Deposition techniques . . . 4
- 1.3 Sputtering deposition system . . . 6
- 1.4 The problem . . . 11
- 1.5 Model Proposed . . . 11
- 1.6 Thesis Organization . . . 14

2 SPUDII: A simulation framework **15**
- 2.1 Architecture . . . 17
  - 2.1.1 The grid . . . 20
- 2.2 SPUDII Modular description . . . 21
  - 2.2.1 TARGSPUD . . . 23
  - 2.2.2 PLASPUD . . . 25
  - 2.2.3 THERMSPUD . . . 31
  - 2.2.4 GROFILMS . . . 37

3 THERMSPUDS2 **39**
- 3.1 Introduction . . . 39
- 3.2 General equation of transport phenomena . . . 42
  - 3.2.1 Transport of energy . . . 43
  - 3.2.2 Transport of mass . . . 45
  - 3.2.3 Transport coefficients . . . 48
  - 3.2.4 Source terms . . . 52
- 3.3 Discretization and method of solution . . . 54
  - 3.3.1 Momentum . . . 61
  - 3.3.2 Boundary conditions . . . 61
  - 3.3.3 Refinement and grid transitions . . . 66
- 3.4 Solution of linear equations . . . 71
  - 3.4.1 Thermalization threshold . . . 73
- 3.5 Algorithm . . . 74
  - 3.5.1 TS2 Algorithm . . . 74
  - 3.5.2 THERMSPUD Algorithm . . . 74

4 Results **77**
4.0.3 Chamber and system configuration 77
4.0.4 External modules 79
4.1 Simulation results 80
4.1.1 Temperature profiles 82
4.1.2 Density profiles 89
4.1.3 Iterative effects on TS2 results 96
4.1.4 Target to substrate distance, effects on TS2 99
4.1.5 Cell size effect 102

5 Conclusions and recommendations **104**
5.1 Conclusions 104
5.1.1 Gas heating effect 105
5.1.2 Rarefaction of background gas 105
5.1.3 Sputtered atoms 106
5.2 Recommendations for future work 106

Bibliography **108**

List of Figures

1.1 Idealized chip 2
1.2 PVD process 3
1.3 Momentum transfer at the target 8
1.4 Sputtering system 9
1.5 Magnetron system 10

2.1 SPUDII structure 17
2.2 2D and 3D discretization schemes 21
2.3 SPUDII and thin film process 22
2.4 Sputtering yield 24
2.5 Real aluminum target 25
2.6 Sheath formation 28
2.7 Interfaces in PLASPUD 32
2.8 THERMSPUD 33

3.1 Transport equation 42
3.2 Minimum target to substrate distance 52
3.3 Finite volume cell 56
3.4 Boundary treatment 63
3.5 Quadtree interfaces 67
3.6 Flux in a quadtree mesh 68
3.7 Interpolation in quatree 69
3.8 TS2 algorithm 75
3.9 THERMSPUD algorithm 76

4.1 Chamber configuration 78
4.2 Erosion profile 80
4.3 XML configuration file 81
4.4 Pressure effect on gas temperature 83
4.5 Power effect on gas temperature 84
4.6 Max temperature as function of power 85
4.7 Max temperature as function of pressure 85
4.8 Experimental temperature reading vs simulation 86
4.9 Hot target 87
4.10 Aluminum vs Copper 88
4.11 Grey scale temperature 88

4.12 3D temperature 89
4.13 Power effect on Ar concentration 90
4.14 Rarefaction as function of power 91
4.15 Rarefaction as function of pressure 92
4.16 Argon density as function of current 93
4.17 Experimental vs simulated argon concentration 93
4.18 Significance of Momentum solver 95
4.19 Rarefaction for Al and Cu 95
4.20 Power effect on Al concentration 97
4.21 Pressure effect on Al concentration 98
4.22 Diffusive and energetic flux 99
4.23 Iterative effects on aluminum deposition 100
4.24 Iteration effect on copper deposition 100
4.25 Effect of different distances on temperature 101
4.26 Effect of different distances on concentration 103
4.27 Cell size effect 103

List of Symbols

TS1	THERMSPUD1
TS2	THERMSPUD2
n_i	Species i density
T	Temperature
P	Pressure
Ar	Argon atom
Ar^+	Argon ion
Ar_{fast}	Energetic argon
m	Mass
S_n	Thermalized particle source term
S_p	Momentum source term
S_e	Energy source term
R^s	Scale factor
e	Electron
e_h	Hot electron density (energetic)
e_c	Cold electron density (thermalized)
i_e	Energetic ion
eV	Electron-Volts
E	Electric field
B	Magnetic field
V	Potential
σ	Collision cross section
σ_i	Collision cross section for species i
λ	Mean free path
λ_i	Mean free path for species i
d	Target-substrate distance
J	Flux
Π_{ij}	Stress tensor
κ	Thermal conductivity
D	Diffusion coefficient
q	Electron charge
I	Current
P_e	Peclet number
$\mathbf{V}$	Average mass velocity in cell
ρ	Density

T	Temperature
Δt	Time step
Δx	Step in x direccion
Δy	Step in y direccion
Δz	Step in z direccion
S	Sticking coefficient
E_{th}	Thermalization threshold
V_{cell}	Cell volume
v_{th}	Thermal velocity
$\bar{c}$	Mean speed of species
c_v	Specific heat at constant volume

Chapter 1

Introduction

1.1 Thin films

Thin films have received a growing interest in recent years due to the ever increasing number of applications for them. The broad scope of applications includes flat panel displays, optical and magnetic coating for storage devices, biological equipment, biotechnology sensors, quantum devices, biological equipment and hardness and decorative coatings. However, the dominant application of thin films is found in the microelectronics industry. Fabrication of any semiconductor device involves the sequential deposition of many layers of materials. The deposition of these materials is a key process of chip manufacturing and determines the performance of the semiconductor device. One of these processes is the metallization stage which refers to the deposition of conductive materials to provide inputs, outputs, power and interconnections to the active devices of an integrated circuit [1]. Figure 1.1 depicts a simplified cross section of a hypothetical chip with 3 levels of metallization showing different layers deposited by standard thin film deposition techniques.

The expression *thin film* is commonly applied to a thin coating less than

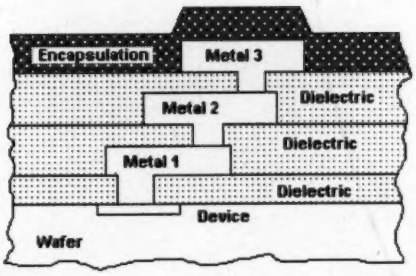

Figure 1.1: **Figure showing a cross section of an idealized chip with three levels of metallization. Different layers of materials as well as vias and contacts can be identified in the figure**

about 1 micrometre in thickness built on top of a substrate by a controlled condensation of individual atomic or molecular species. This thin layer can completely transform the characteristics of the substrate. The special and distinctive properties of thin films are not only the result of their thickness but also of the internal structure of the film as a result of the process of building the film atom by atom [2]. Optical, magnetic, electrical, chemical, mechanical and thermal properties of thin films are different from those properties commonly founded in the bulk material and they are frequently enhanced by this special deposition process.

Any thin film deposition process can be divided in 3 major steps: production of the precursor atomic species, transport to the substrate and condensation or reaction on the substrate [2]. Figure 1.2 summarizes these processes listing some of the principle variables for each case.

The source of depositing species may come from a solid, liquid or vapor material. The main characteristic which determines the organization for thin film deposition techniques is the difference in the production process of these

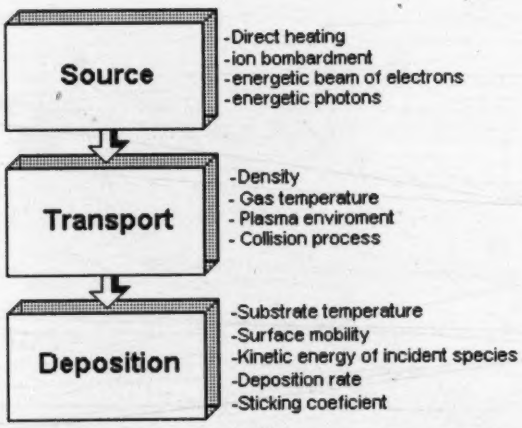

Figure 1.2: **Three principal block stages in which a Physical Vapor Deposition (PVD) process is normally divided. Each stage involves a different physical process and it can be decoupled from each other**

source species. For instance, the depositing source can be obtained by direct heating of the source material in its solid state or it can come from a chemical reaction.

Once the atomic or molecular precursor species are created, they are transported to the substrate. This process is normally conducted under a vacuum environment in order to reduce contamination and to increase the transport efficiency of the flux. The use of a vacuum environment reduces the number of collisions between source and residual gas particles. The mean free path, the average distance a particle travels between collisions, is inversely proportional to gas density. Therefore, in a low gas density environment, source particles undergo fewer collisions and arrive at the substrate with significantly higher energy depending on the process. This scattering affects film properties and deposition rate [3].

Finally, the condensation step on the substrate determines various prop-

erties of the film. This has several stages: nucleation or island formation, island growth, agglomeration and filling. First, the impinging particle hits the substrate and is physically adsorbed. The particle which is not strongly bound to the substrate tends to be desorbed at a certain rate. If the rate at which particles arrive at the substrate is greater than that at which they are desorbed, these particles start to aggregate and eventually they form small islands which are in thermal equilibrium with the substrate. This process is known as the nucleation stage. These islands continue to grow until they start to merge with each other forming a film with some unfilled spaces. The latter process is known as agglomeration or coalescence [2]. Finally, if the atoms are mobile enough to diffuse and if they fill these remaining holes, a relatively continuous film is formed. Diffusion is enhanced if the temperature of the process or the energy of the particles is increased. On the other hand, if the atoms at the surface do not diffuse to cover the unfilled spaces, a columnar structure is grown.

1.2 Deposition techniques

Vacuum coating started over a century ago when an understanding of the micro and nano world was very limited. The methods available at that time were a product of persistent experiments rather than theoretical understanding.

There are two main techniques used to deposit a thin film: vapor phase deposition and liquid phase deposition. However, most films are deposited using a vapor phase deposition technique. Some of the advantages of vapor phase deposition over liquid phase deposition includes applicability to more materials, flexibility in substrate temperature and access to the surface during deposition [2].

The vapor phase deposition techniques can be clustered into two groups: Chemical Vapor Deposition (CVD) and Physical Vapor Deposition (PVD). A major difference between these two techniques is the way the vapor source of the material to be deposited is produced. In PVD techniques, the vapor source comes from a solid material while in CVD techniques the vapor source derives from a gaseous or liquid chemical precursor. In addition, in PVD both vapor transport and deposition occur by physical processes, although in some cases a simple chemical reaction may occur at the substrate [2]. The choice of PVD over CVD as a method to deposit thin films depends on the applications and the desired properties of the film. Properties such as adhesion and surface mobility increase with increasing temperature. Unfortunately, a high temperature substrate is not always compatible with other materials or requirements of the system. For example, heat is not always desired in metallization since this enhances diffusion of dopants and undesired materials into the semiconductor device changing the characteristics of the chip. PVD films are typically deposited at lower temperatures even though some improvements in CVD techniques have allowed lower temperature deposition processes. Both PVD and CVD techniques have been used for decades in microelectronic fabrication where CVD processes are more related to the deposition of dielectric and polysilicon layers and PVD techniques are more commonly used in the metallization stage. Improved understanding and control of PVD techniques is required to optimize associated process variables to obtain the desired film properties.

The several techniques found in PVD can be grouped into two main categories: evaporation and sputtering. As mentioned before, the metallization stage is one of the most critical steps in the construction of a chip. Metallization includes the deposition of diffusion barriers, seed layers, interconnection

and contact layers. These films are required to have good step coverage on steep, sub-micron structures and high uniformity over large Si wafers [4]. Sputtering typically produces better step coverage than evaporation principally because higher energy particles hit the substrate enhancing film condensation. Nowadays, with the advent of Cu contacts (Cu is electroplated rather than sputtered) sputtering has been slowly replaced for metalization. However, sputtering is still critical in the formation of seed layers, diffusion barriers and contact silicides.

1.3 Sputtering deposition system

Sputter deposition is a very popular and efficient way to deposit thin films of different materials on a variety of substrates. For example, this basic process is used to metallize integrated circuits, to create transparent thin films, produce optical coatings and to form high-density magnetic and magneto-optical coatings. There are 4 main reasons that explain why a sputtering system is used instead of other depositions systems: Compatibility, which means different materials can be deposited onto a variety of substrates; flexibility, implying that there are many different variations of the basic process (which allows for a variety of processes to exist); control, there are many controllable variables which can change the film properties; and quality, which implies that dense films can be grown with reasonable coverage over nonplanar substrates [1].

The use of the term sputtering to describe this technique has been a subject of controversy over the years. J.J. Thompson introduced the term *spluttering* in 1913 but then I. Langmuir and K.H. Kingdom eliminated the 'l' in their subsequent publications. Since then, this once *electrical evaporation* or *cathode disintegration* technique has been known as sputtering [5].

Sputtering was first studied by W.R. Groove in 1852, but this effect was probably observed before he did by other people who were also interested in glow discharge phenomena. He noticed that when a metallic wire was placed in a vacuum chamber and a glow discharge was created, the material of the wire was somehow ejected from its surface and was deposited on the inner walls of the chamber. He only could see this effect when the metallic wire was the cathode of the circuit. This inexplicable phenomena was primarily used at that time to produce mirrors, since the quality of mirrors being made by this *electrical evaporation* machine was superior to those made by other vacuum coating methods available at that time.

Basically, a sputtering system consists in a chamber at low pressure where a plasma is created by means of ionizing gas atoms [6]. Ar is primarily used because it is inert, cheap, abundant and moderately heavy. Two main bodies can be identified within the chamber: the target and the substrate. The target is the source of the material to deposit and the substrate is any surface onto which the target material is going to be deposited. The argon ions are attracted by a high negative bias applied to the target (typical values ranges from -300 to -1000 V).

When an ion approaches a solid surface, a number of possible interactions between the surface and approaching ion can be identified: the ion may be reflected after neutralization with a significant fraction of its incident energy, the ion can cause the ejection of an electron from the target, the ion may be implanted in the target (ion implantation), the ions can modify the structure of the target or it may dislodge some of the atoms in the surface via cascade collisions due to transference of momentum. It is the latter effect which is known as sputtering and it is our interest to investigate it. The resulting effect depends on several factors such as the energy of the ion, voltage of the

surface, target material, angle of incidence, crystal structure of the surface and the binding energy of the target material [7]. The momentum transfer mechanism is showed in figure 1.3. In this process, some of the ionized Ar atoms hit the target surface, gaining an electron, being reflected as neutrals. Both the sputtered and the reflected neutrals are important to the development of the film.

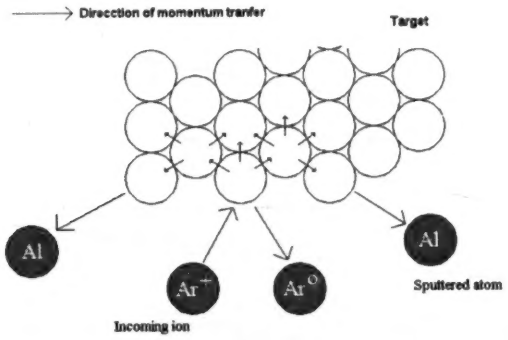

Figure 1.3: **Arrows show the momentum transfer mechanism at the target when it is struck by an energetic ion. Through a series of collisions, some surface atoms may be ejected.**

The simple configuration depicted in figure 1.4 is known as a diode sputtering system. This is the basic sputtering structure found in the literature. The diode configuration is inefficient because the electrons emitted from the target are quickly lost to the anode and hence are not available to ionize the gas and sustain the plasma. As a result, high voltages are required (typical values range from -500 to -5000 V); high pressures are needed, increasing collisions in the plasma region (30 to 120 mTorr), reducing the energy of sputtered atoms on their way to the substrate; and electron bombardment at the substrate is increased causing heating in the film. An improvement for the diode sputtering system is triode sputtering where a filament provides extra electrons to sustain the plasma resulting in a reduced operating pressure and voltage. The

main problem with this configuration is that the filament is very sensitive and it is damaged quite easy [4].

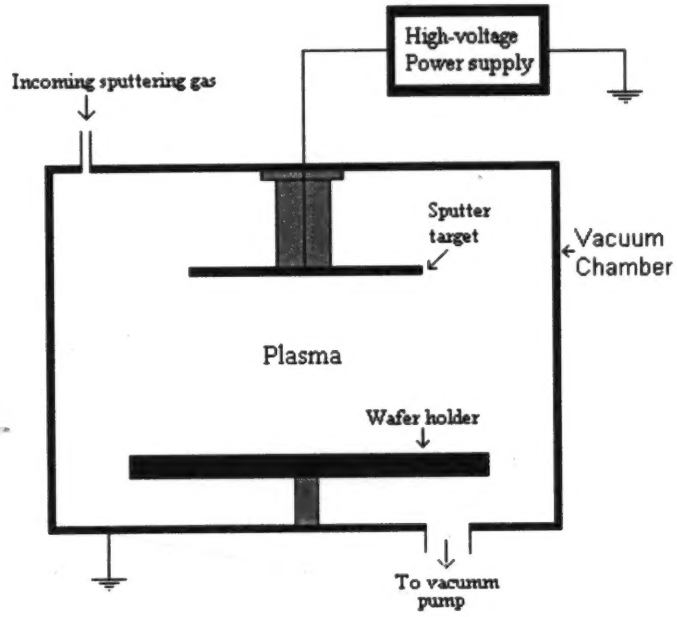

Figure 1.4: **A typical sputtering system. The target is powered by a high voltage power supply. The plasma is localized between target and substrate. Sputtering gas in introduced in order to maintain a constant pressure inside the chamber.**

The sputtering method most commonly used is magnetron sputtering. This technique has a higher deposition rate, a higher film density and lower substrate heating than conventional diode sputtering. In this configuration, the secondary electrons ejected from the cathode are confined by magnets placed behind the target. This allows operation at lower pressures (3 to 30 mTorr) and lower voltages (200 to 500 V) than the diode sputter method. Operation at lower pressures means a higher mean free path which implies a reduction in collision events between sputtered and gas particles. This reduction leads to

a flux of higher energy sputtered particles at the substrate, improving properties of the film such as adhesion, surface roughness, density and coverage. Increasing the energy of the sputtered species has a similar effect to increasing the temperature of the process. Figure 1.5 shows a simplified picture of a dc magnetron sputtering system.

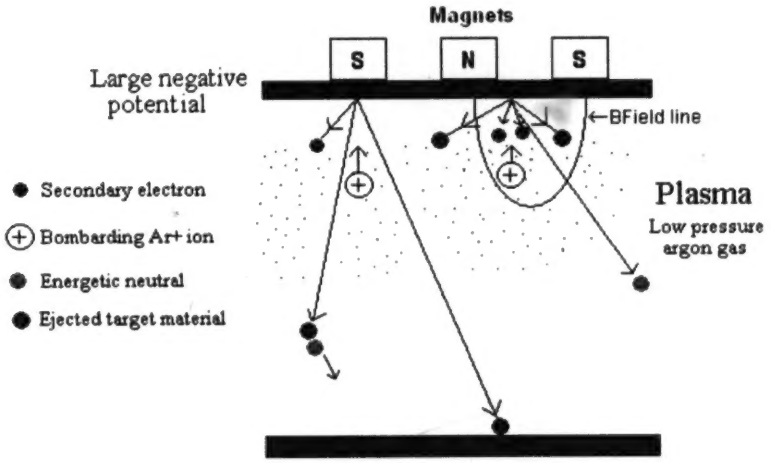

Figure 1.5: **Typical magnetron sputter system. Magnets above the target confine electrons and enhance plasma density. Electrons are confined and follows elliptical trajectories in this region.**

Pioneering work done on sputtering by Stuart and Wehner showed that the minimum energy required to cause sputtering is roughly four times the heat of sublimation of the material, an energy referred to as the sputtering threshold [7]. The number of atoms sputtered from the target for each impinging ion is known as the sputtering yield. It depends on target material, ion energy, ion type and surface morphology. This is a very important process variable in sputtering. For instance, the deposition rate, which is the rate at which a film is formed in the substrate, is a function of the sputtering yield. Typical sputtering yields ranges from 0.1 to 3.

1.4 The problem

When traveling through the chamber, energetic neutrals may undergo several collisions with background gas particles, and, as a result of these collisions, they lose some or all of their initial kinetic energy. Properties and microstructure of the film depend on several factors such as the flux of atoms, ions and neutrals at the surface of the substrate and their energy. For instance, reflected neutrals can produce 4 different kinds of effects that contribute to the microstructure of the film: implantation, peening, energy for enhancing diffusion and resputtering [1]. Because of all of the variables involved and all the effects they have on the film grown, it is crucial to have a complete understanding of transport processes. A comprehensive theoretical model for sputtering has not been well defined due to the complexity of the process, and computational tools are therefore essential to simulate the effect of process variables on the final microstructure of the film and thereby reduce the high cost of experimental process development. For these reasons this work presents a simulation study of the transport process of sputter deposition.

1.5 Model Proposed

A hybrid scheme is proposed which solves for the transport of neutrals within the chamber of a magnetron sputtering system, where neutrals refers to the neutralized reflected ions, sputtered, gas or metastable atoms. This hybrid scheme, THERMSPUD, will be part of a new application framework for comprehensive reactor-scale PVD simulation named SPUDII. Versatility, reuse, extensibility and ease of use are only some of the key characteristics of this framework. In addition, it is sufficiently efficient to allow execution on a desktop workstation. This project is a complete replacement for the SIMSPUD

program, a reactor-scale PVD simulator that has been extensively used to simulate PVD deposition. SIMPSUD has been successfully commercialized and sold all over the world during its lifetime. However, it was constrained to homogeneous conditions which are not generally applicable to typical deposition conditions [8].

SPUDII is divided in 4 principal modules, each one working in an specific task. The modules are designed to be as independent entities as possible. One of these modules is THERMSPUD. THERMSPUD is a hybrid model and is split up into two sub-modules: THERMSPUD1 (TS1) and THERMSPUD2 (TS2). The former deals with the transport of energetic neutrals while the latter solves for the transport of thermalized neutral particles. In TS1, a collision of energetic particles is simulated using a Monte Carlo (MC) method following a soft-collision model. As soon as a particle has been thermalized, it is sent to TS2 to be processed. Making reference to figure 1.2, THERMSPUD2 would be enclosed in the transport box. In TS2, the proposed model solves coupled diffusion and heat conduction equations in a continuum formulation on a 3D grid to obtain spatial distributions of gas density and temperature within the chamber of a magnetron sputtering system. This thesis focuses on developing and implementing the TS2 sub-module. It is necessary to mention that the TS1 module already exists in the framework. Therefore TS2 will follow the communication protocol established when TS1 was first written.

Recently, a number of simulations trying to numerically solve the transport of energetic and thermalized neutrals in a glow discharge have been reported in various scientific publications. Despite of the fact that some of these simulations are on plasma environments different to that normally found in a magnetron system [9–11], they provide an insight to the effects some process variables have in the rarefaction and gas heating measurements reported

elsewhere [12–16]. Magnetron simulations are frequently done in a one or two dimensional grid due to the complexity of the processes and they are mostly based on a Monte Carlo (MC) method. These simulations usually utilize a number of simplifications in order to reduce the execution time inherent in Monte Carlo algorithms and are focused on trying to determine one individual aspect of a very complicated process. One common simplification is to neglect changes in the background gas temperature and density caused by the sputtered neutrals or the plasma species. Furthermore, most of the simulations reported so far use a simplified fixed geometry which limits the scope and versatility of the software. The model proposed overcomes these limitations using an innovative framework where it is possible to reconfigure the chamber geometry at run time [8].

Thermalization of sputtered neutrals in a glow discharge has been investigated in several scientific publications [17–28]. Other papers explore this same process but do not provide a thermalization profile for sputtered and reflected energetic particles using a non MC approach [29–31]. Valles-Abarca *et al.* [23] explored beyond thermalization of neutral species and tried to simulate the transport of thermalized particles using a diffusion equation. They used a continuous energy loss approximation to obtain the average kinetic energy of thermalized particles as a function of distance to the cathode using an elastic collision model. This approximation is used as a source term for the steady-state diffusion equation. In this way they obtained a spatial distribution of thermalized atoms.

The phenomena of gas heating in a glow discharge has also been investigated and reported in several publications. According to these studies, a gas heating effect has been observed in the plasma region next to the cathode surface. This effect has been either obtained by direct measurement meth-

ods [13, 15, 16] or simulated via solution of the heat equation with a power input from a collision module [22, 32, 33]. As a common methodology to simulate this complex process, the energetic neutral transport module is decoupled with the heat conduction solver. This scheme is extended by means of coupling heat, mass and momentum solver for thermalized particles with a high energetic transport module. The principal difference between the simulators developed so far and the THERMSPUD module will be explained in greater detail when this module is outlined in the next chapters.

1.6 Thesis Organization

The present work is organized in 5 chapters. Chapter 2 explores some of the most important aspects of SPUDII. This chapter will provide a global picture of the framework architecture and module interdependence and the role they play in the simulation. It will also explore the basic features of the framework on which almost all the remaining work is based. Chapter 3 deals with the central part of this work: the design, implementation and construction of THERMSPUD2, the module in charge of the transport of thermalized particles. It also explains some key features of the algorithm and methodologies chosen to solve the governing diffusion equations. A brief explanation of the key functions in the module is also provided. Chapter 4 will provide some results obtained by TS2 as an independent simulation module as well as when it is used in conjunction with TS1. Finally, Chapter 5 summarizes the work done and explores some of the possible modifications to the model and propose some ideas to overcome some of the software's limitations for future work. A brief discussion of some possible improvements is also included.

Chapter 2

SPUDII: A simulation framework

The SPUDII suite of simulators is a result of a natural evolution of the SIMSPUD simulator. SIMSPUD is a PVD simulator which solves for transport of neutrals in a homogeneous PVD process chamber. This software gives spatial flux density distributions and angular and energy distributions of particles arriving at the substrate [1]. SIMSPUD can be used in conjunction with a feature scale simulator to accurately simulate film growth at any surface. For instance, SIMSPUD is usually used with SIMBAD to simulate the final microstructure and density of the film. SIMSPUD has been a very successful simulator that was commercialized by the Alberta Microelectronic Corporation (now Micralyne) and Reaction Design. This simulator has been principally used in the microelectronics industry as a tool to simulate metallization of new materials for developing new technologies (ionized PVD). During the years, this research tool has been object of numerous extensions to increase its reuse and functionality. It has also had to be adapted to new chamber configurations and gas environments. As a result of all these changes and improvements, SIMSPUD had reached its reusability limit and the point where it cannot be easily up-

dated any more without restructuring the code.

SPUDII evolved from the need for a more extensible and flexible reactor scale simulator for PVD deposition. Rather than being a single simulator, SPUDII is a suite of simulators that encompass the simulation of the whole sputter deposition process. The goal of SPUDII is to be as flexible, extensible and efficient as possible. Ideally, this would execute on a desktop workstation. These characteristics are difficult to find in a single simulator when simulating complicated physical processes such as sputtering. Frequently, powerful simulators can only be run on supercomputers due to the extensive number of operations that are needed in order to achieve a solution. This, as one can expect, increases the cost of simulation tools which reduces their appeal.

Most of the time, scientists are more interested in the understanding of a specific aspect of a more complex or sometimes unexplained process. When they build a computational model to simulate this behavior they are more focused on solving that specific problem, neglecting the effect that other variables have in the system. For instance, in sputtering it is common to see variables such as pressure or gas temperature to be held constant through the course of the whole simulation process. Taking these variables as constants limits the number of real applications these simulators can perform to those experiments that resemble these specific characteristics.

A detailed description of the SPUDII framework is found in [8] and the reader interested in a more in-depth explanation is referred to this document. However, a general description of this framework is necessary in order to have a big picture of SPUDII and be able to understand the place TS2 plays in the whole project. Therefore, a general description of SPUDII modules and its basic architecture features is provided in the next pages in order to set the ground for the upcoming chapters.

2.1 Architecture

SPUDII is built using an object-oriented methodology with C++ as the language development tool. SPUDII simulates the three main stages depicted in figure 1.2 by means of a modular architecture. This modular methodology is made feasible by ensuring that every major aspect of the deposition process is decoupled to be simulated individually. SPUDII is a novel model proposed as a means to build a more detailed simulator for PVD deposition. SPUDII uses a more sophisticated and complete approach. This software has 4 main modules, each one concentrating on one specific chore. A simplified block diagram of this software is depicted in figure 2.1.

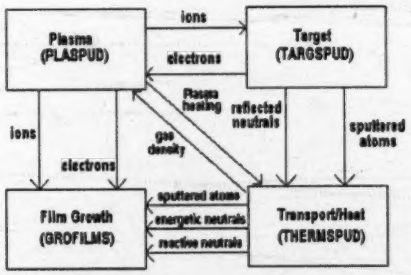

Figure 2.1: **Internal structure of the SPUDII suite of simulators. Each block represent a module. Lines depict the internal relation and interdependencies between modules. Each module is designed to be as independent as possible from each other.**

The whole SPUDII framework is encapsulated within a Simulation Object which creates, runs and destroys all the objects needed in the simulation. As a requirement for being a framework, it is necessary that all these objects are tied together as loosely as possible. Consequently, the Simulation Object is in charge of handling all the objects and as well as creating an architecture within which all modules can operate[8]. The simulation object can create three types

of object: ExecutionModule, ProcessModule and LowLevelModules.

All the ExecutionModules are independent units and they do not rely explicitly on any other module. An execution module has the ability to initiate and perform an execution phase in the simulation [8]. When communication between modules is needed, it is performed using interfaces. This allows the Simulation Object to have an architecture where the ExecutionModules do not explicitly depend on another module to be executed. Each module can be initialized independently in the XML configuration file and it is not a requirement of the simulation to create the other ExecutionModules. Within the simulation, only one instance of an execution module can exist at one time.

A ProcessModule is the next module in the object hierarchy. A ProcessModule provides a service to any ExecutionModule that requires it. These modules, as opposed to ExecutionModules, have to be owned by other objects to be properly initialized. Ownership and initialization parameters entries is done in the XML configuration file. Several kinds of ProcessModules can be included in the simulation provided that they are owned by different ExecutionModules.

Finally, a LowLevelObject is any object which is not required to have any ownership. These kind of objects are handled as normal objects are in C++: Vectors, Particles, Points, Cells. These specific kind of objects do not need to be initialized in the XML file.

One of the most common problems faced in computer modeling is to decide how input and output parameters should be handled. In modeling physical processes, such as sputtering, there are several simulation parameters which are required to perform a single simulation. Target voltage, pressure in the chamber, geometry of the chamber, target-substrate distance are just some

of the user defined parameters that the simulator needs to know in order to be executed. Furthermore, if at one determined point of the development process it is required to add one or more parameters to the framework, usually it involves a substantial amount of work which is commonly solved by *hard coding* a value. This solution requires a rebuild for each change and it promotes the spreading of *magic numbers* throughout the code [8]. A similar problem is faced when one wants to obtain valid output data for its analysis using another computational tool.

Configuration file

SPUDII overcomes the problems of configuration, output and input managing and ownership using an architecture where data is managed using a text-based data storage file standard. The standard chosen to be used in SPUDII was XML (extensible markup language). The exact process in which the information is extracted from the XML file (a process that includes the creation of Document Object Module files) is complicated and beyond the scope of this work to explain; it is enough to say that the data entered in the XML file is loaded in the simulator without the need of recompiling the whole project. All variables are configured using one single XML file at run time.

The XML file is also the main configuration file. The user can add or delete modules, changing the whole simulation, only by means of editing a single XML file. It is also possible to avoid modular initialization saving valuable time when doing a set of simulations by means of this file. SPUDII's architecture allows a relatively easy configuration to resemble a specific user application at run time.

2.1.1 The grid

One of the most important characteristics of a simulator is the representation and discretization of the simulation space. This discretization is a critical step for a continuous model where a set of PDE's are numerically solved to simulate the physical process which is described by these equations. This is typically done through some grid which stores variable values at a representative discrete set of points. The field that deals with discretization and grid generation issues is rather complicated, and it is becoming more important in present times as powerful desktop stations are becoming more accessible for scientists. There is practically no limit to the number of ways a physical region can be divided, starting from the typical cartesian discretization to the most complicated and sophisticated logarithmic adaptive grid. The choice of the discretization grid depends on the physical process to simulate and the dimensions of the physical domain. If the physical domain has symmetry in one coordinate system, it is clear that a mesh that uses this coordinates system is the best choice. If, on the other hand, one expects that the solution would have a greater gradient in a determined region of the apparatus, one can choose a mesh that reflects this assumption, i.e. a logarithmic mesh. But, if one expects indeed a solution with a greater gradient in a determined zone but without a clear idea about the location of this zone, the grid has to be able to adapt itself according to the solution by performing a local refinement in that zone.

As mentioned before, one of the key features of SPUDII is the adaptability to any chamber configuration. It follows then that the kind of grid that best suits SPUDII is an adaptive grid. A three-dimensional quadtree mesh commonly known as octree was the chosen grid model. This decision was made based on previous experience with these type of meshes. Quadtrees and octrees have been reported to be very efficient for continuum approaches [34–38].

An octree is a special kind of grid where the physical region is first divided in a predetermined number of cubes. After a refinement criteria has been reached, the grid refines itself only in those regions that require refinement. The cell is then divided in eight small cells as shown in figure 2.2.

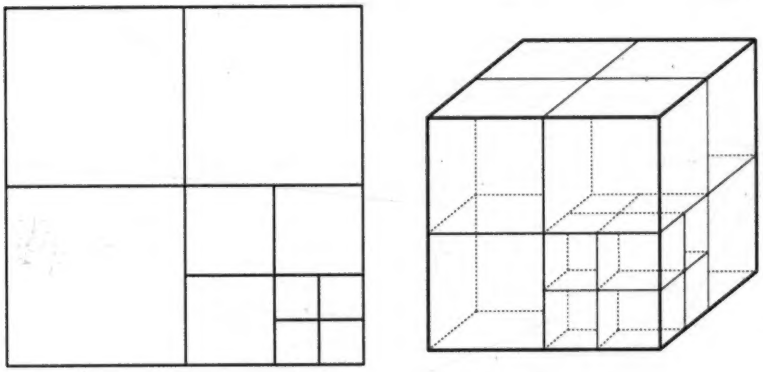

(a) Quadtree (b) Octree

Figure 2.2: **Grid discretization with refinement. (a) shows a two-dimensional mesh refinement scheme known as quadtree. An octree is obtained if the quadtree is extended to three dimensions. In an octree every cell is refined in 8 child cells as shown in (b)**

The use of an octree requires special treatment at those regions where a grid transition is localized. This will be explained in the next chapter.

2.2 SPUDII Modular description

The strength of SPUDII resides in its modular architecture. Each module works in a different part of the process and it performs a specific task. For instance, PLASPUD deals with plasma simulation while TARGSPUD simulates the physics of the target's interaction with ions, GROFILMS is responsible

for the simulation of film microstructure and properties and THERMSPUD is responsible for simulating heat conduction and transport of neutrals from target to substrate. Comparing to figure 1.2, the relationship between SPUDII's modules with the stages of thin film deposition is depicted in figure 2.3.

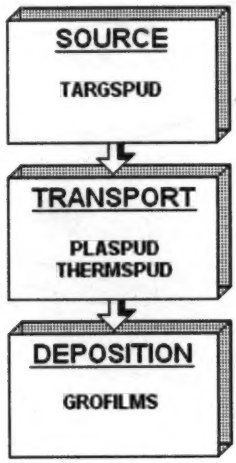

Figure 2.3: **SPUDII and the thin film process. Each model works in a specific part of the film deposition process and can be individually initialized depending on the application**

There is a great deal of complexity associated with each on these components. These processes are a complicated succession of events in dynamic equilibrium and even a small change in one variable can produce a cascade of effects leading to a significant change in the whole system. Nevertheless, in an attempt to provide a solid background for subsequent chapter development, a brief explanation of each module is given in the remainder of this chapter emphasizing the physical processes that govern the phenomenon that the module simulates. Additionally, a brief and simplified discussion of some physical laws related to each module is provided. Emphasis is made in the relation between these phenomena and neutral densities since TS2, the module which is the fo-

cus of this thesis, is responsible for supplying density and temperature profiles to every other module.

2.2.1 TARGSPUD

Probably the only module of SPUDII that is not directly linked to TS2 is TARGSPUD. TARGSPUD simulates the events at the target as a result of ion bombardment to provide other modules with sputtering distributions of atoms ejected from the target. TARGSPUD receives as input a flux of ions striking the target and it returns angular and energy distributions of energetic neutrals and sputtered atoms. It is also a source of secondary electrons for sustaining the plasma [39].

One of the most important variables related to the target is the sputtering yield. As was stated before, the sputtering yield is the average number of atoms sputtered from the surface of the target per incident ion. This significant ratio is influenced by some factors such as surface contamination, target materials, energy of incident particles, angle of incidence of particles and crystal structures of the target surface [7]. It can be seen elsewhere [2, 3, 7, 39] that the sputtering yield increases with increasing ion energy almost linearly until it reaches a plateau and starts to diminish. At this energy, ions start to implant rather than cause collision cascades at the target surface. This plateau is commonly observed at ~10 keV. There is also a minimum energy threshold for the ion to cause a sputtering event. As a result, a useful energy range for ions to produce sputtering can be identified: from sputtering threshold (roughly $15 \sim 30$ eV) to the plateau energy ($10 \sim 100$ keV). Figure 2.4 shows the energy dependence of sputtering yield for a hypothetical/typical target material.

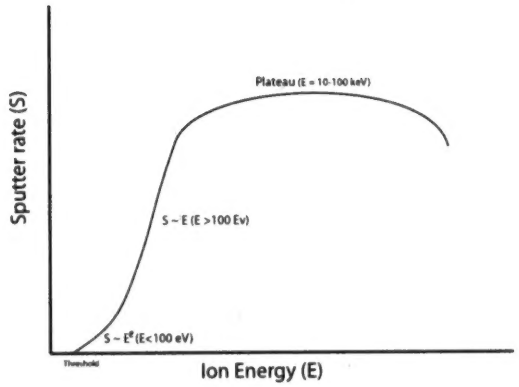

Figure 2.4: **Dependence of sputtering yield with energy of incoming ion. Three zones can be identified: the low energy zone where no sputtering occur (below the sputtering threshold), the sputtering zone where yield varies almost linearly with energy and the high energy zone where atoms are rather being implanted than causing sputtering.**

The standard model used to simulate events at the target is the theoretical model developed by Thompson [40] for the energy and angular distribution for sputtered atoms. The ejection of atoms is assumed to be a result of a collision cascade product of ion bombardment. This theory is only valid at high energies when ions penetrate sufficiently deeply into the target to interact with a large number of atoms [1]. Other authors use a cosine distribution to determine the angular distributions of sputtered atoms as a complement to Thompson energy distributions. TARGSPUD uses a model where 'master equations' for ion and particle transport in solids are numerically solved to obtain energy and angular distributions for the sputtered particles. This model accounts for ion-target and target-target collisions which are the basic interactions that occur at the target surface in sputtering (ion-target collisions and momentum

transfer).

Interactions at the target are especially difficult to simulate in magnetron discharges. Rather than having uniform erosion at the target, commonly non-uniform erosion profiles are seen as a product of magnetic electron confinement. This confinement produces a localized ionization region meaning that the target is being bombarded by a non-uniform flux of ions. A photograph of an erosion profile of an aluminum target from a magnetron system can be seen in figure 2.5. Note the typical racetrack erosion profile found in magnetron targets.

Figure 2.5: **Photograph of an aluminum target from a magnetron sputtering system. The non-uniform erosion profile is a product of electron confinement due to magnets placed behind the target.**

2.2.2 PLASPUD

Glow discharge plasma phenomena was first observed by the 17th century scientist Jean Picard (Picard's glow) in the evacuated tube of a mercury barometer. Since then, there has been a number of studies to understand the complexity of glow discharges and the spectral emissions from the glow [5].

The vacuum tubes led various researchers to investigate ionized gases more conscientiously. The use of the term *plasma* to refer a partially ionized gas is attributed to I. Langmuir [5]. In general terms, a plasma is a partially or fully ionized gas which is created when energetic particles collide with gas atoms releasing one or more of the electrons bound to the atom, ionizing it positively. The minimum energy for an atom to be ionized is known as the ionization energy. For argon, which is the most common gas used in glow discharges like the ones used in the thin film industry, this ionization energy is $15.68eV$. It is also possible to ionize atoms by a multiple collision mechanism known as step ionization. Usually, energetic electrons are the colliding particles to create the plasma. Electrons are easy to energize using electric fields and relatively easy to confine in an specific region using magnetic fields, permitting a more easily controlled process. Since additional electrons result from the ionization process, good efficiency can be realized.

Energetic electrons or *hot electrons* e_h, are created near the cathode and move away toward the wall as a result of electric field. On their way they collide with atoms which they may ionize. After scattering, they continue on their path and may suffer additional collisions until they are lost to the walls of the chamber. Generally, electrons are quickly lost before many ionizations can occur. However, if a magnetic field exists in the region close to where they were created, they will be spatially confined undergoing multiple collisions and ionizing several gas atoms if they still posses enough energy to do so. When an electron has lost most of its initial energy due to collisions, it is considered as thermalized and is part of the *cold electron* e_c group. It is important to notice that not all the collision events result in an ionized atom. Elastic collisions and excitation events are just some other processes that can also be a result of the interaction between these colliding particles. As a matter of fact, the

characteristic glow of plasmas is principally due to relaxation of excited atoms after a collision with an electron.

Two main regions can be identified in a typical dc glow discharge: a dark and a glowing zone. The former zone is typically known as the positive column zone while the latter is known as the negative glow. The mechanisms that lead to the formation of these zones are complex but they can be summarized as follows. Assuming that the plasma exists and it is at equilibrium, then a sheath is formed when a substrate (floating or energized) is put inside the plasma being bombarded by a flux of electrons and ions. Since electrons are lighter than ions they move faster in the medium, tending to strike the substrate more frequently which biases the substrate negatively with respect to the plasma. This negative potential has the effect of repelling electrons which reduces their flux until an equilibrium is reached. This net electron accumulation at the substrate leaves behind positive ions creating a sheath of net positive charge around it. Figure 2.6 depicts a simplified voltage distribution in a typical dc glow discharge. Note that there is practically no electric field in the negative zone (equipotential zone).

PLASPUD is the module that is in charge of plasma simulation. PLASPUD is a hybrid approach consisting of a fluid model and a 3-dimensional Monte Carlo solver working together. Basically, PLASPUD divides the plasma into energetic and thermalized particles, and transport of these particles is simulated in different stages. The current design of PLASPUD have 3 sub-modules: PS1, PS2 and PCHEM.

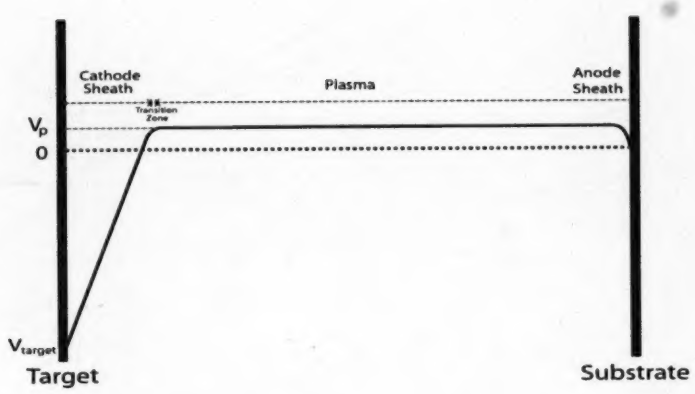

Figure 2.6: **Potential distribution in a glow discharge. Sheath and plasma regions can be identified. From [39]**

PLASPUD1 (PS1)

As stated before, PS1 solves transport of hot electrons, e_h and energetic ions, i_e. One of the services that PS1 provides is energy and density distributions of hot electrons and energetic ions. It also provides PS2 with the source terms for the solution of continuity and Poisson equations. PS1 performs such tasks using a MC model to solve for the equations of motion for energetic charged particles within the chamber. A charged particle being affected by electric and magnetic fields moves according to the Lorentz force equation:

$$m\frac{d\mathbf{v}}{dt} = q(\mathbf{E} + \mathbf{v} \times \mathbf{B}) \tag{2.1}$$

where m is the particle mass, $\mathbf{v}$ is the particle velocity, q is the particles charge, $\mathbf{E}$ is the electric field and $\mathbf{B}$ is the magnetic field at the location of the particle [39]. $\mathbf{B}$ is static and calculated at the beginning of the simulation using

an external solver. Given **E** and **B**, PS1 numerically solves the Lorenz force differential equation for the particle under consideration. Particles are tracked during a time step after which a calculation is performed to decide whether or not a collision event has taken place. To determine this, PS1 makes a call to PCHEM which randomly decides based on the weighted cross sections of the input energetic processes. To perform such calculations, PCHEM needs the neutral density vector and the temperature in that specific region. The neutral density vector allows the simulation of multi-gas species environments. PS1 provides PCHEM with the neutral density vector which in turn is obtained from the TS2 grid. After a collision event has been determined, PCHEM provides PS1 with the kind of collision event. As soon as PS1 knows the type of collision, PS1 performs the operations related to this event and continues to track this particle until it is outside the plasma sheath. PS1 also checks if the particle's energy has dropped below the thermalization threshold. This value is commonly taken as the minimum energy to have any kind of relevant event (minimum excitation energy) and it can be configured at the beginning of the simulation. Ions and electrons outside the sheath which fall below the threshold are transfered to PS2 and it uses them to compute local creation rates of thermalized particles.

Other services provided by PS1, which are loosely linked to TS2, include Electron Energy Distribution Functions (EEDF) and spatial distribution of densities of hot electrons. This information could be used for a more complete analysis for the heat source in TS2. This will be discussed in the next chapter.

PLASPUD2 (PS2)

PS2 is a sub-module that receives thermalized electrons and ions as source terms from PS1 and solves continuity equations for them. PS2 also solves for

plasma potential using Poisson's equation. In PS2, transport of thermalized electrons and ions is solved by treating these particles as a fluid and solving coupled continuity equations. As commented earlier, a plasma is formed of charged and neutral particles in dynamic equilibrium. Since the negative glow region is practically equipotential, movement of particles does not follow any prescribed path and their transport is believed to be governed by collision events. Only electrons, which are lighter than ions, can respond to weak electric fields existing in the transition region close to the sheath and as a result of this they have a tendency to move away from the cathode. In the equipotential plasma zone, ions are believed to reach the sheath edge by diffusion. When they are in contact with the sheath they are quickly accelerated to the cathode due to the high potential gradient in the sheath region.

To solve fluid equations for ions end electrons, PS2 needs to calculate some thermalized macrostate variables which reflect, in average, plasma behavior such as collision rates. To do so, PS2 calls PCHEM asking for these values. PCHEM is in charge of providing PS2 with these important parameters which then are used to solve the continuity equation. PS2 can communicate directly with TS2 to obtain the necessary neutral information using an independent interface or it can be connected indirectly using PCHEM as a communication module.

PLASCHEM

PCHEM provides collision outcomes to PS1 and collision frequencies to PS2. It is also the sub-module that decides if an energetic charged particle has undergone a collision and the kind of collision process that has occurred every Δt step in PS1. This is the only module which is aware of the various energetic processes that occur in the plasma.

First, when PS1 calls PCHEM to determine if a collision has taken place, it weights all process cross sections with their respective neutral density to obtain a probability of collision. Then it generates a random number to decide whether a collision has taken place or not. If there has not been a collision, PS1 continues tracking the particle for another time step.

Another service that is provided by PCHEM is the calculation of collision frequencies which are used in PS2 to determine the transport coefficients for the solution of the continuity equation for thermalized ions and electrons.

Interfaces

When two modules or sub-modules need to communicate, the communication is performed via an interface. There are two interfaces which are extensively used in PLASPUD sub-modules to communicate with TS2: IDensity and INeutralGas. The use of INeutralGas and IDensity interfaces allow PLASPUD sub-modules to be as independent as possible. This architecture also keeps circular dependencies (file 'a' depends on file 'b' and file 'b' depends on file 'a') to a minimum and helps keep the project file organization under control [8]. PCHEM depends on TS2 to obtain the density vector but TS2 does not depend on PCHEM to execute. Figure 2.7 shows how PLASPUD communicates with TS2 using INeutral and IDensity interfaces.

2.2.3 THERMSPUD

Transport of particles in a gas has been intensively investigated over the years. This transport process is important for the development of the film during deposition since the flux and energy of atoms hitting the substrate strongly depends on the mechanism by which the atoms from the target are transported

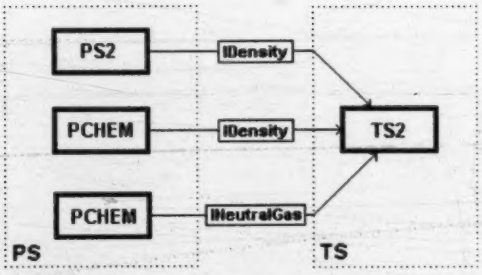

Figure 2.7: **Interfaces being used by PLASPUD to communicate with TS2 to process information relevant to each module. Each interface is configured in the XML file to point to TS2.**

to the substrate. As one can expect, if the medium in which the atoms are moving is a low density gas, which is the case for sputtering, the importance of collisions is determined by the pressure regime. Collisions are an efficient method (depending on relative masses) of energy transfer, and they are important since even a small number of them can transfer significant momentum and energy to the gas. Unfortunately, sputtering processes commonly take place in a regime known as transition or Knudsen flow making difficult to generalize whether many or almost no collisions occur [1].

THERMSPUD, the neutral transport/heat module, is a hybrid model which solves for the transport of neutrals within a magnetron sputtering system. Due to the complexity of the process, most of the previous investigations have been performed making several simplifications. For instance, they have assumed a homogeneous gas density and have neglected the gas heating effect. Also, the interatomic potential used to obtain cross sections and scattering parameters is based either on a hard-sphere scattering model or on elastic collisions which neglect long range interactions between atoms. Additionally, most of them do not incorporate a plasma module, thereby ignoring the effects that plasma

interactions have in the transport of neutrals. Other approaches that simulate the rarefaction and gas heating effect use a simplified model to perform this simulation. THERMSPUD is divided into two sub-modules: TS1 and TS2. The former is a MC simulation of energetic neutrals based on a soft-collision model and the latter is a fluid model of thermalized particles and heat conduction based on a continuum approach to solve for gas rarefaction and gas heating. Figure 2.8 depicts the internal structure of THERMSPUD.

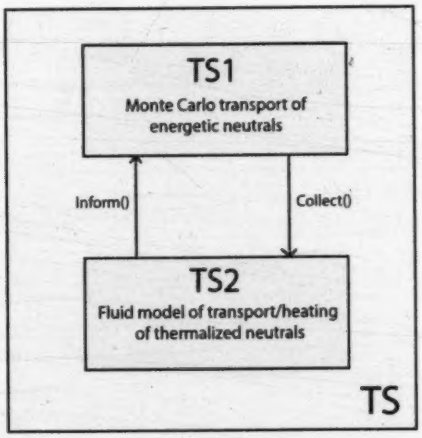

Figure 2.8: **Internal structure of THERMSPUD. Each module communicates with the other using interfaces to keep dependencies at minimum. TS1 and TS2 iterate indefinitely until TS2 sends a 'stop' signal to TS1 indicating it has converged.**

After thermalization, particle transport is generally governed by diffusion. The approach used to solve for the transport of neutrals within the chamber is similar to the one proposed by Valles-Abarca *et al* [23].

THERMSPUD1 (TS1)

TS1 is a more sophisticated version of SIMSPUD. As mentioned before, SIMSPUD is a three-dimensional Monte Carlo vapor transport simulator. Monte Carlo simulation of scattered process is the standard approach to modeling this process at typical operating pressures. MC simulations keep track of every single particle and are based on the generation of random numbers to determine the final particle's direction after a collision has occurred. SIMSPUD uses a hard sphere model where atoms are considered to be solid spheres which interact between each other. In general terms, SIMSPUD follows energetic particles on their way from the target to the substrate assuming they undergo elastic collisions with background gas particles. The initial energy distribution of sputtered particles is obtained from the model developed by Thompson [40] while the angular distribution can be any arbitrary empirical emission function. The distance a particle travels before a collision, λ, is obtained from a Poisson distribution:

$$f_\lambda = \frac{d\lambda}{\lambda_m} e^{-\lambda/\lambda_m} \tag{2.2}$$

where the mean free path λ_m is function of the collision cross section σ. Robinson [41] observed that σ is energy dependent and its value is approximated using a power law. The energy lost in the collision is then approximated using an expression derived from classical collision theory. This scheme ignores long-range particle interactions and is based on an empirical cross-section parameter. The scattering angle is obtained assuming a hard sphere model. Also, SIMSPUD assumes a uniform density and temperature within the chamber.

Like SIMSPUD, TS1 tracks particles in straight line trajectories between

collisions to see if they strike the walls or substrate. On the other hand, TS1 tracks only until particles become thermalized and can be treated by TS2. It is believed that a more realistic and efficient treatment of energetic neutral atoms can be obtained following this approach. One of the main problems of MC simulations is the time spent in tracking down a large number of particles particularly the thermalized ones which, on average, have stabilized energies. This is particularly important if a more realistic inhomogeneous gas is to be handled since trajectories then have to be stepped to sample local conditions. To surmount this problem, it is proposed to divide the flux of neutrals in energetic and thermalized fluxes. Following this approach, TS1 only works with energetic particles depositing in TS2 all particles that have fallen below a pre-determined energy value as a result of numerous collisions. The key features of TS1 that differentiate it from SIMSPUD are [8]:

- A more physically based collision cross-section model
- A soft potential scattering model
- Multiple gas species support
- An improved apparatus shadowing model
- Inhomogeneous gas density and temperature

The scattering and cross sections for collision events have been observed to be energy dependent. For this reason, there is a need for obtaining an interatomic potential that accounts for large range interactions between atoms. The interatomic potentials that have been previously used are derived from Robinson [18, 20, 24, 29] or some interpolation scheme based on it [17, 42]. Some authors use an average scattering angle depending on the energy lost in the collision [25] or have neglected scattering events [30]. Other authors have reported the use of more sophisticated schemes where long-range interactions have been included, i.e. interpolated Abrahmson potential model [27, 33, 43],

interpolated Leonard-Jones potential [21], Moliere potential [19] or Thomas-Fermi-Morse potential [26]. Leonard and Dew [8] proposed a scheme where an inelastic collision model using a soft potential approach based in the ZBL interatomic potential mode is used. TS1 uses the model proposed by Ziegler *et al.* (Ziegler Biersack Littmark interatomic potential) and the so-called *magic formula* to obtain collision cross sections and scattering angles for each collision. The magic formula provides the basis for TS1's scattering model [8]. The way TS1 simulates collision events is not that different from SIMSPUD method. A mean free path is obtained from a Poisson distribution similar to 2.2 where λ_m is obtained from:

$$\lambda_m = \frac{1}{\sum_{i=n_o}^{n} n_i \sigma_i} \tag{2.3}$$

The difference between λ_m in SIMSPUD and the one used in TS1 is that the latter can handle multi species environments within the chamber while the former is only valid for two species. TS1 handles inhomogeneity using a pseudo inhomogeneous gas density model where the chamber is divided into a grid and uniform gas density and temperature are assumed within each individual cell. Density and temperature in each cell are upgraded after every global iteration as a means to handle gas rarefaction. Since every cell has a different density and temperature, every time a particle goes from one cell to another, a new λ_m has to be calculated. If multiple gas species simulation is performed, a weighted average neutral density data structure extracted from the current cell is used to determine randomly the appropriate species of the gas particle with which the particle has collided [8].

TS1 tracks energetic particles during their life time until they reach the substrate (deposition), hit the walls or become thermalized. Once the particle

has been deposited somewhere, TS1 continues to track more particles until they reach a thermalization limit. This thermalization limit is set in the TS2 XML file. TS1 will stop when it has generated an amount of thermalized particles equal to this limit and global convergence of THERMSPUD is finally attained.

THERMSPUD2 (TS2)

TS2 solves transport equations for thermalized neutral particles. The analysis, formulation and solution of this sub-module is the main contribution of this thesis and is covered in the next chapter.

2.2.4 GROFILMS

GROFILMS (GRain Oriented FILm Microstructre Simulator) is a 2D simulator that simulates the condensation and growth of thin films. GROFILMS is the successor of SIMBAD (SIMulation by BAllistic Deposition) developed at the University of Alberta. Properties such as grain size, column orientation and surface roughness depends on factors such as energy of incoming atoms, angle of deposition, temperature and pressure. For instance, for a given set of parameters, flatter films can be grown if the temperature of the process is increased. High energy deposition atoms are desired for obtaining a more uniform and dense film. However, as was pointed out before, high temperature processes are not desired for metallization.

Condensation of thin films on top of the substrate is not an easy issue and it is not completely understood yet. It involves a number of intricate processes which are determined by a set of variables that influence the characteristics of the film. In addition, these variables depend strongly on each other and

even a small variation in one of them can result in a dynamic change in the condensation stage. The variables that have the most effect in the development of the film are substrate temperature, angle of incidence of the flux and energy of incoming particles.

It was stated before that temperature affects variables such as mobility of particles and desorption. Nucleation is strongly dependent in both parameters and a realistic simulation must be based as much as possible on accurate models taking in consideration these important variables. The flux of atoms striking the substrate is also of importance since it affects the nucleation and filling stages of deposition as well as shadowing effects. The incidence angle also plays an important role in the development of the film. The probability that a particle will stick to a surface is greater, for a particular energy of incidence, if the particle hits the substrate at normal incidence than if it hits it with an oblique angle. This effects is more pronounced at high energies (>15 eV).

GROFILMS has a substantially different architecture than SIMSPUD. GROFILMS was written in C while SPUDII is written in C++. This difference implies that for GROFILMS to run using SPUDII architecture and communication protocols, some modifications have to be done in its code. Specifically, an entry for the extra information provided by SPUDII modules was developed for GROFILMS to properly run in conjunction with SPUDII.

Chapter 3

THERMSPUDS2

3.1 Introduction

Numerical solution is a powerful tool used to reveal various behaviours that other methods can not explore. Nowadays, the increasing performance and relatively low price of computers have allowed to scientists to entertain numerical simulations of more complex phenomena in an attempt to have a better understanding of the physics of phenomena in the everyday world.

THERMSPUD2 is a numerical solver for steady state convection plus diffusion and heat conduction equations for thermalized particles in a sputter deposition system. As previously mentioned, thermalized particles are defined as those which, after several collisions, have their energy below a certain energy threshold. Once thermalized, their transport is simulated by a fluid model rather than a molecular approach. In TS2, transport equations for these particles are solved in a non-uniform grid (octree mesh) with anisotropic transport coefficients in a multi-gas species environment. These conditions are typically found in most dc magnetron sputter deposition systems used in industry and research.

Several attempts have been made in an effort to obtain a more realistic model for neutral transport and gas heating in sputtering systems. In the majority of these models, people use the background gas as a buffer for the energetic particles module as a common simplification (the background particles are somehow forgotten after a collision). This means that the gas density and temperature is taken as uniform everywhere. However, an important rarefaction effect has been found to exist principally between the cathode and the substrate of most systems based on plasmas. Experimental measurements of density in a sputtering system have confirmed that the background density of the sputtering gas is not uniform [15, 16, 44]. This effect was first explained to be caused by the sputtering wind [44], the flux of energetic neutral particles coming from the target (sputtered atoms and reflected neutrals). This energetic flux heats the filling gas transferring energy to it as a product of the collisions between energetic neutral particles and gas atoms. In considering this effect, rarefaction and gas heating of the filling gas need to be coupled with a high energy transport model (TS1) to have a more realistic simulation. The main reason that rarefaction and heating affect energetic neutral transport is because the mean free path of an energetic particle is a strong function of the local density and temperature of the filling gas. Furthermore, these parameter also impact the plasma characteristics necessitating their incorporation into the plasma module (PLASPUD). In SPUDII, rarefaction and gas heating effects are simulated by coupling TS2 with TS1 and PLASPUD [1].

As can be noticed in figure 2.1, THERMSPUD is an important submodule of SPUDII. TS1 and TS2, together, form a hybrid approach to solve for transport of neutral particles. TS2 receives source term information information from TS1 and indicates when to stop the execution of TS1. This stop signal is

[1]See chapter 2

normally sent when TS2 has received enough particles to have a representative statistical ensemble of thermalization events. Once TS1 and TS2 have converged, THERSMPUD inputs to GROFILMS the energy and particle fluxes for it to start a film growth simulation.

Neutral and energy flux at the substrates of sputtering systems are parameters which determine the final microstructure and quality of the deposited film. These atomic and energetic fluxes are difficult to obtain using analytical methods due to the complexity of the process. Additionally, the complex geometry of magnetrons and the pressure regime (Knudsen flow) where most systems work make it difficult to obtain a general analytical solution. For these and other reasons already explained, it is imperative to use computational simulation and numerical methods to approximate these fluxes.

Numerical solution of most physical problems normally involves three main steps:

1. Formulation of the appropriate mathematical expressions that adequately describe the physics of the problem (commonly Partial Differential Equations or PDEs).
2. Discretization of the continuous domain into a finite number of localized points or volumes using algebraic approximations.
3. Solution of the system of algebraic equations obtained after discretization.

This chapter follows a similar order to the one listed above. First, the basic transport equations for diffusion of matter and energy are derived. The validity and applicability of these equations are subject to several basic assumptions to adequately describe the transport phenomena. Second, discretization of the transport equations is tackled using a finite difference treatment for the diffusion-convection equation. Spacing of the resulting grid determines the accuracy and the cost of the computation. Boundary conditions (Dirichlet

and Neumann) are solved at each chamber feature using simple assumptions. Transport coefficients for heat conduction and diffusion of matter are approximated following a simple hard sphere model due to the low energy regime of interest. Refinement is handled using a model for octree meshes where tetrahedral linear interpolation is applied to obtain values of density and temperature at points other than the center of the cells. Finally, a set of linear equations is solved using an iterative scheme to handle refinement and weak nonlinearities of the transport coefficients.

3.2 General equation of transport phenomena

Transport of a specific property ϕ in a medium is normally described using PDE's. The general equation for transport phenomena [45] is given by:

$$\frac{\partial \rho\phi}{\partial t} - div(\rho\phi\mathbf{V}) = div(\Gamma\ \nabla\rho\phi) + S_\phi(x, y, z, t) \tag{3.1}$$

where ρ is the density, ϕ some specific property, Γ the transport coeffieient, $\mathbf{V}$ the local velocity field and S_ϕ the generation rate of property ϕ.

These 4 terms can be associated with physical processes as shown in fig 3.1. The quantities ϕ of interest are temperature, concentration, velocity, etc.

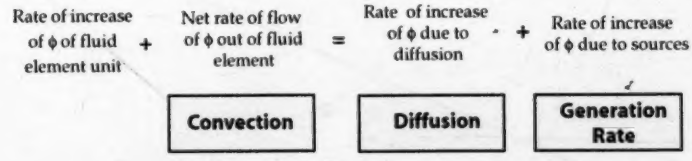
Rate of increase of ϕ of fluid element unit
+
Net rate of flow of ϕ out of fluid element
=
Rate of increase of ϕ due to diffusion
+
Rate of increase of ϕ due to sources
Convection
Diffusion
Generation Rate

Figure 3.1: **Conceptual interpretation of the terms in the general transport equation (equation 3.1)**

3.2.1 Transport of energy

For the pressures typically employed for sputtering, it is common to find convection, as a mechanism of heat transport, to be neglected. This means that the energy transport phenomena is normally assumed to be dominated by a conduction mechanisms. Examples of this assumption for the sputtering process include [15, 16, 22, 29, 33]. Urbassek and Sibold [29] argue that convective energy transport is negligible (less than 5%). Serikov and Nanbu [33] neglected the convective term based on the numerical value of Peclet's number P_e (the ratio between the convective term, diffusion term and cell's size). In their work, it is argued that the small value of P_e obtained under conditions normally found in a sputtering chamber indicates a predominantly conduction mechanisms process. Turner [22] also followed this assumption and neglected convection to obtain gas temperature profiles. It is also possible to add a convection term in the energy equation to investigate with more detail the effect of convective transport. However, this addition represents a more complicated problem since it is uncertain what convective velocity to use. There are as well some other glow discharge simulations [9–11] where heat conduction is assumed to be the predominant mechanism for heat transport in the filling gas. Therefore, following these approaches and for the sake of simplicity, TS2 also uses a model where convection is neglected.

Dropping the time dependent term to focus on the steady state solution and neglecting convection, equation 3.1 transforms to:

$$div(\Gamma \nabla\phi) + S_\phi(x, y, z) = 0 \tag{3.2}$$

or, in terms of the heat flux:

$$div(J_\phi) + S_\phi(x, y, z) = 0 \tag{3.3}$$

where J_ϕ is the total flux due to energy dissipation and $S_\phi(x, y, z)$ is the energy generation rate.

J_ϕ can be approximated by Fourier's law of heat conduction. Fourier's law reads [46]:

$$J = -\kappa \nabla T \tag{3.4}$$

where κ stands for the thermal conductivity of the medium and T is its temperature.

Substituting equation 3.4 into 3.3 gives:

$$div(\kappa \, \nabla T) + S_T(x, y, z) = 0 \tag{3.5}$$

The background gas is being heated due to several energy sources during deposition in a non-uniform manner. Arguably the most important sources are those ones involving collisions with energetic particles originating at the target. Other heat sources that contribute to gas heating are from the plasma (ionization and excitation, electron collisions, radiation) and from hot objects such as hot substrates and heating walls. However, in TS2, it is assumed that the dominant source factor for energy transport is the flux of energetic neutrals. From the plasma, electrons are believed to not contribute significantly in the heat generation term as their mass is negligible when compared to that of ions and atoms. Ions, on the other hand, are massive enough to be considered in the simulation. However, neutral density is several orders of magnitude ($\sim$ 3 or 4) higher than that of ions, which in turn justifies neglecting any collisions involving ions for the time being. Bogaerts *et al* [9] reported results that validate these assumptions. Even though they refer to conditions different from sputtering, their results validates this approximation as an initial approach. Some of the modules that provide energy generation rates to TS2 are not

fully functional yet. The model proposed is easily extended to accept other generation rates from other modules once they are completed.

3.2.2 Transport of mass

Diffusion is an ubiquitous process. The simplest mathematical model of diffusion was first developed by Fick in 1887 based on the thermal conduction theory derived by Fourier years before. Diffusion is caused by random molecular motion that leads to complete mixing [47]. Considering particles diffusing in a gas, their transport can be describe by means of their local concentration n_i. This concentration is function of the coordinates x, y and z as well as time. Concentration varies spatially because of sources and sinks in the chamber and because the gas is heated in a non-uniform manner. For these reasons, the dependence of n_i is not straightforward.

Particle flux can be split into two components. The first component is due to concentration gradients that drives molecules away from zones of high concentration to less concentrated zones (the diffusion term), and the second component which is due to a mass average velocity that moves particles as a result of a collective behavior (the convective term). The convective term is believed to play an important role in the steady state concentration profile of the filling gas and it should not be neglected when simulating gas and pumping flow [44].

The simplest model to describe particle diffusion is to use Fick's law to approximate this phenomena. Fick's first law of diffusion relates the flux of particles with a gradient of concentration. This equation reads [47]:

$$J_{dif} = -D\nabla n_i \tag{3.6}$$

where D stands for the diffusion coefficient and n_i is the number of molecules

per unit volume.

For the convective term, the flux due to a mass average velocity, J_{conv}, is approximated using [47]:

$$J_{conv} = n_i \mathbf{V} \tag{3.7}$$

with $\mathbf{V}$ being the average drift velocity per cell.

Substituting equation 3.6 and 3.7 in 3.1 and neglecting the time derivative for the steady state solution yields:

$$div(n\mathbf{V}) = div(D\,\nabla n) + S_n(x, y, z) \tag{3.8}$$

To solve equation 3.8, one needs the velocity $\mathbf{V}$ field. To obtain this equation, 3.7 should be coupled with a momentum equation that solves for this average velocity. However, such a coupled system is difficult due to the complexity of the stress tensor. Fortunately, one can simplify the stress tensor for an inert gas reducing considerably the complexity of the equations.

The full momentum equation reads [48]:

$$\frac{\partial}{\partial t}(\rho\mathbf{V}) + \nabla \cdot \rho\mathbf{V}\mathbf{V} = \rho S_p - \nabla P + \nabla \cdot \Pi_{ij} \tag{3.9}$$

where ρ is the mass density per cell, $\mathbf{V}$ the cell velocity field, S_p the momentum generation rate, P the pressure field and Π_{ij} the stress tensor.

For a newtonian fluid, equation 3.9 in steady state is reduced to [45]:

$$\nabla(\rho u\mathbf{V}) = \nabla(\mu \nabla u) - \frac{\partial P}{\partial x} + S_{p_x} \tag{3.10}$$

$$\nabla(\rho v\mathbf{V}) = \nabla(\mu \nabla v) - \frac{\partial P}{\partial y} + S_{p_y} \tag{3.11}$$

$$\nabla(\rho w\mathbf{V}) = \nabla(\mu \nabla w) - \frac{\partial P}{\partial z} + S_{p_z} \tag{3.12}$$

where u, v and w are respectively the x, y and z components of the velocity field and S_{p_y} is the "total" momentum generation rate for the i component of **V**.

Solving the last system gives a velocity field which in turn is introduced in equation 3.8 to solve for the diffusion and convection of thermalized particles.

As a final comment, TS2 also receives its momentum source term from the TS1 module. Each thermalized particle being added to the TS2 grid also deposits a part of its momentum into the cell.

The diffusion-convection equation only holds provided that some assumptions are considered. A number of limitations can be identified but three of them are the most important ones. These three basic assumptions that are required for equation 3.8 to apply in solving this particular problem are:

- Distances considered are large compared with λ.
- All particles have the same velocity but different directions of motion; after each collision the particles change their directions randomly.
- Concentrations do not change abruptly from place to place.

If one of these assumptions is not met, the continuity equation is not valid to describe diffusion. From the list, the most important simplification is the one involving λ. In magnetron systems it is common to find different configurations with different target to substrate distances. These distances have been optimized experimentally to obtain the best quality and the desired characteristics of the films being deposited. This particular issue will be addressed later in the work.

Note the similarity between equations 3.5, 3.8 and 3.10. All of them look similar in structure with some minor differences and, as a first guess, one

could contemplate on using the same method to explode this resemblance. However, as will be addressed later in this work, equations 3.8 and 3.10 are not straightforward to discretize, and they have to be treated carefully to avoid numerical divergence.

3.2.3 Transport coefficients

To properly discretize equations 3.5 and 3.8, one requires proper expressions to approximate the corresponding transport coefficients, namely κ, D and μ. These variables summarize the collective behavior of particles in a single coefficient. It is desired to have a single expression to obtain these coefficients because of their non-linear nature.

The easiest expressions that can be used to obtain these three important parameters are derived from the viscosity coefficient expression first developed by Maxwell [49]. These simple expressions for the transport coefficients read:

$$\mu = \frac{1}{3}\rho\lambda\bar{c} \tag{3.13}$$

$$\kappa = \frac{1}{3}\rho c_v \lambda\bar{c} \tag{3.14}$$

$$D = \frac{1}{3}\lambda\bar{c} \tag{3.15}$$

where c_v in the specific heat at constant volume and $\bar{c}$ the *mean speed of species*.

The numerical value of these coefficients strongly depends on the collision cross-section model used to obtain λ (remember equation 2.3). As was addressed before, Robinson [41] noted that σ is energy dependent, with this

dependence being more pronounced at high energies ($> 1eV$) since long range interactions influence the collision process. In a later work, Phelps *et al* [50] obtained values of cross sections for Ar-Ar collisions for a broad range of energies. In this paper values of cross sections are compared with the ones used in [51]. Additionally, it is showed that extrapolation from Robinson theory for high energy values results in smaller cross sections than the ones obtained here. Due to the fact that there is practically no full data on viscosity coefficients for most metals in inert gases, and to the fact that this work is concentrated only on Ar-Ar collisions, the latter model is not viable to use in TS2.

Thermalized particles, which are the focus of this work, are defined to have at most 9 times the thermal energy [2]. As a first approximation, a more general approach based on a hard sphere model is use to approximate σ in the energy range of interest for TS2. Indeed, it was noted that the hard sphere model is a very good approximation for cross sections in the low energy regime used in TS2 [26], if the diameters of the atoms are properly selected. Therefore, the hard sphere model is used to approximate σ in TS2. This model can be further improved to investigate the effect that different cross section models have in the transport phenomena.

The hard sphere model assumes molecules to be small spheres of diameter d_i. In the simplest case, assuming only species 1 and 2, σ_{12}, the collision cross section for species 1 and 2, is obtained via:

$$\sigma_{12} = \frac{\pi(d_1 + d_2)^2}{4} \tag{3.16}$$

Equation 3.16 can be multiplied by a correction factor to obtain values closer to the ones obtained in [50], but this would be only valid for Ar-Ar collisions. Further investigation could lead to a more appropriate expression

[2] See subsection 3.4.1

for σ if experimental data becomes available for comparison.

Equation 3.15 can be improved to approximate its theoretical value to experimental data [49] using the Chapman-Enskog theory. Substituting $\bar{c}$ into 3.15 and after some corrections to the $\frac{1}{3}$ and the mean free path expressions, for the simple case of only 2 species, equation 3.15 finally reads:

$$D = \frac{3}{8}\sqrt{\frac{\pi}{2}}\frac{1}{n\lambda_{12}}\left(\frac{m_1 + m_2}{m_1 m_2}kT\right)^{1/2} \tag{3.17}$$

m_1 and m_2 being the masses of species 1 and 2. This equation is used as an approximation to calculate D in [52].

For the thermal conductivity κ, a similar correction procedure [49] applied to equation 3.14 leads to:

$$\kappa = \frac{25\pi}{64}\rho v \lambda_{vc} c_v \tag{3.18}$$

where λ_{vc} is the *Mean free path for viscosity and heat conduction* [49] and is equal to:

$$\lambda_{vc} = \frac{1}{\sqrt{2}\sigma_{12} n} \tag{3.19}$$

For a mixture of gases, the simple mixture rule holds for most of the cases. Assuming that there are only two neutral species inside the chamber, the sputtering gas Ar and the target material Al, the total thermal conductivity κ_{tot} of the mixture reads:

$$\kappa_{tot} = k_{Ar}\frac{n_{Ar}}{n_{tot}} + \kappa_{Al}\frac{n_{Al}}{n_{tot}} \tag{3.20}$$

The TS2 heat conduction solver uses equation 3.20 to calculate the thermal conductivity coefficient for a mixture of gases. Further simplification derives in:

$$\kappa_{tot} \approx \kappa_{Ar} \tag{3.21}$$

since $n_{Ar} \gg n_{Al}$ even for high sputtering rates. In case of reactive sputtering, equation 3.20 should be changed to take account of the cross section ratios and different densities.

According to equation 3.18, anisotropic thermal conductivity makes equation 3.5 a non-linear differential equation. In contrast to other works [9, 15, 22, 33] where κ is held constant, TS2 solves for non constant κ. In [10], a very similar expression for κ is used to solve heat conduction in a two-dimensional analysis.

For the sake of simplicity, the viscosity coefficient was taken as constant based on the fact that it was assumed that the main contribution in the momentum equation is due to the pressure field and momentum sources. The numerical value of the viscosity is derived from 3.10. For argon:

$$\mu = 2.5 \times 10^{-5} \frac{Ns}{m^2} \tag{3.22}$$

One could argue that this is a crude simplification, but the low value of the viscosity for real gases looks like a good reason to avoid the extra computational effort to solve for a non-uniform viscosity.

As a final remark on transport coefficients, it is necessary to comment about the validity of the diffusion equation given a target to substrate distance, d. As pointed in subsection 3.2.2, if this distance is comparable to the value of λ at some relevant pressure, the diffusion equation starts to break down and is not valid to describe transport phenomena. This restriction is by far the most critical for this work. The minimum d can be approximated assuming that it follows the expression $d \gtrapprox 3\lambda$. For a hard sphere model, a crude estimation for d gives:

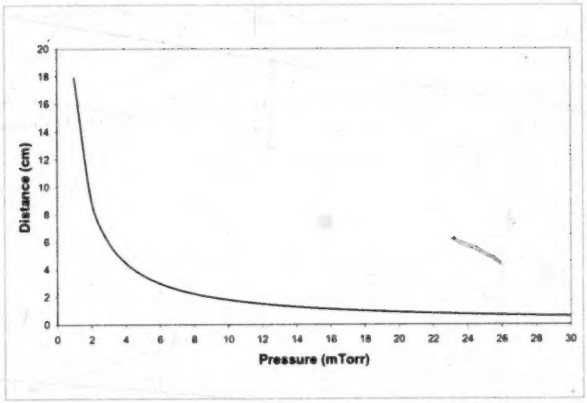

Figure 3.2: **Dependence of minimum target to substrate distance on the system pressure. Depending on the pressure, the TS2 solver is valid when the target to substrate distance is bigger than the value suggested by equation 3.23.**

$$d \gtrapprox \frac{22.5}{\sqrt{2}} \frac{kT}{P\sigma} \tag{3.23}$$

where P is the system pressure in $mTorr$.

In figure 3.2, equation 3.23 is plotted as a function of Pressure. It should be noted that typical systems have $P \approx 1 - 50mTorr$ and $d \approx 5 - 20cm$. Therefore, these assumptions are valid for most but not all sputter systems. Once a specific configuration is defined one should consider figure 3.2 to be sure that TS2 is working in an applicable region.

3.2.4 Source terms

As commented earlier, TS2 receives source particles, energy and momentum on a per cell basis from TS1. Every cell holds a variable for the number of thermalized particles N_t and the amount of energy deposited E_t due to

collisions during the execution of TS1.

The final expressions for the particle source S_n, momentum source S_{p_i} and energy generation S_e terms are:

$$S_n = \frac{N_t R^s}{V_{cell}} \tag{3.24}$$

$$S_{p_i} = \frac{m v_i R^s}{V_{cell}} \tag{3.25}$$

$$S_e = \frac{E_t R^s}{V_{cell}} \tag{3.26}$$

where V_{cell} is the volume of the cell, v_i is the x,y or z component of the particle velocity, and R^s is the rate scale needed to obtain real generation rates from the number of sampled particles.

The rate scale is the ratio between the number of real particles to the number of simulated ones per unit time and is defined as:

$$R^s = \frac{\Lambda I}{q N_s} \tag{3.27}$$

where I is the target current, q the electronic charge, N_s the total number of energetic particles simulated in TS1 and Λ could be either the sputtering yield or the reflection probability, depending on the kind of neutral particle.

Both reflected and sputtered neutral fluxes can be seen as two different particle generators on a surface. Every time a particle is created in the target, the target manager randomly selects a particle generator to create a new particle. These particle generators are weighted according to the ratio between the sputtering yield and the reflection probability. After TS1 is finished, TS2 obtains from TS1 a single value for R^s.

It can be noticed that increasing the number of simulated particles in TS1 decreases R^s which in turn increases the accuracy of the simulation. In doing this, one is sacrificing accuracy for computation time. There is a minimum

value of simulated particles which will give a statistical validation of the simulation. This value depends on several factors such as geometry, pressure, target-substrate distance; its value is more likely to be found experimentally. For the case study of next chapter, this value was found to be $\approx 8 \times 10^5$.

3.3 Discretization and method of solution

The model proposed divides the chamber in rectangular parallelepiped cells, which can be locally refined as needed. For each cell, transport equations are discretized based on standard finite differences using the finite volume method. Solving for concentration of species i plus temperature is performed in an iterative scheme due to the non-linear nature of equations 3.8 and 3.5. As the solution proceeds, an estimate of local truncation error at all grid points is calculated until this error is smaller than a predetermined value signaling convergence.

Several methods exist for the solution of partial differential equations, most commonly finite difference, finite element, MonteCarlo and recently Tranmission Line Matrix. These methods have differences from each other and are a challenge to be programmed in a computer. The method chosen in this work to numerically solve equations 3.5 and 3.8 was the finite volume or control volume method. This method is a special case of finite differences and is extensively used in the Computational Fluid Dynamics field.

The decision to use this method was based on several factors:

- Simple discretization scheme suitable for the diffusion and heat equation in a 3D mesh [45, 53]
- SPUDII cell discretization compatible with the finite volume method [8]

- Suitable sweeping functions for the Gauss-Seidel approach
- Relatively easy handling of boundary conditions [45]
- Easiest and simple method to solve nonlinear diffusion [45, 53]
- Weak non-linearities in thermal conductivity and diffusion coefficient
- An acceptable initial guess is easy to obtain

The chamber is discretized in small cells and finite volume equations are solved in a per cell basis. A set of algebraic equations is then obtained and solved iteratively using a non-linear Gauss-Seidel approach with SOR acceleration.

Heat conduction

To illustrate the use of the finite volume method to solve the heat conduction recall equation 3.5 in 3 dimensions:

$$div(J) + S_e(x, y, z) = 0 \tag{3.28}$$

The finite volume method is based on volume integration of equation 3.28 over the cell as shown in [45, 53]. Using an uniform grid, one can define κ_e and κ_w as the interface conductivities following the convention showed in figure 3.3 (uppercase letters refer to values at the center of cell while lowercase letters refer to values at the interfaces between cells). Using well known central differences to discretize equation 3.28 and making $S_E = 0$ leads to:

$$\frac{J_e - J_w}{\Delta x} + \frac{J_n - J_s}{\Delta y} + \frac{J_f - J_b}{\Delta z} = 0 \tag{3.29}$$

Substituting equation 3.4 into 3.29 leads to:

$$a_P T_C = a_E T_E + a_W T_W + a_N T_N + a_S T_S + a_F T_F + a_B T_B \tag{3.30}$$

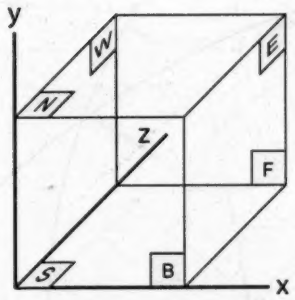

E=East W=West N=North S=South F=Front B=Back

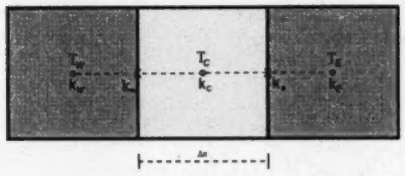

Figure 3.3: **Cell for finite volume method in a uniform grid. The interface thermal conductivities κ_e and κ_w are needed in order to properly discretize equation 3.28 using the finite volume method**

where

$$a_E = \frac{\kappa_w}{\Delta x^2},\ a_W = \frac{\kappa_e}{\Delta x^2},\ a_N = \frac{\kappa_n}{\Delta y^2},$$
$$a_S = \frac{\kappa_s}{\Delta y^2},\ a_F = \frac{\kappa_f}{\Delta z^2},\ a_B = \frac{\kappa_b}{\Delta z^2}$$
$$a_P = a_W + a_E + a_N + a_S + a_F + a_B \tag{3.31}$$

and the interface conductivities are linearly interpolated as:

$$\kappa_e = \frac{\kappa_C + \kappa_E}{2}, \kappa_w = \frac{\kappa_C + \kappa_W}{2}, \kappa_n = \frac{\kappa_C + \kappa_N}{2},$$
$$\kappa_s = \frac{\kappa_C + \kappa_S}{2},\ \kappa_f = \frac{\kappa_C + \kappa_F}{2}, \kappa_b = \frac{\kappa_C + \kappa_B}{2} \tag{3.32}$$

Solving for T_C assuming a cubic cell where ($\Delta x = \Delta y = \Delta z$) and isotropic κ gives:

$$T_C = \frac{1}{6}\left(T_E + T_W + T_N + T_S + T_F + T_B\right) \tag{3.33}$$

Algorithm 3.33 is the well known layout of the heat equation for a uniform 3D grid with isotropic thermal conductivity. This algorithm is applied to every cell in the grid in following a predetermined sweeping order and the new value of the dependent variable is obtained in terms of its known neighbors. The solution evolves starting with an initial guess assuming starting values of n and T for every cell in the grid. This procedure is commonly known as the Jacobi method.

Depending on the sweeping direction, the convergence rate can be improved if values previously calculated are used in the the actual calculation. For instance, if the grid is swept from left to right, the value of the left neighbor is already known because it was calculated in the previous cell. Following this

approach, the convergence rate can be considerably improved. This method is commonly known as the Gauss-Seidel iteration, the algorithm for which reads:

$$n_c^{\overline{k+1}} = \left(T_E^k + T_W^{k+1} + T_N^k + T_S^{k+1} + T_F^k + T_B^{k+1}\right) \tag{3.34}$$

where k stands for iteration step ($k+1$ is the actual iteration step).

Diffusion

Direct use of central differencing and linear interpolation to discretize equation 3.8 leads to numerical problems in certain cases. To illustrate this case, equation 3.8 is discretized with the same method used in last section.

Equation 3.8 in 1D without sources reads:

$$\frac{d}{dx}(n\mathbf{u}) = \frac{d}{dx}(D\,\nabla n) \tag{3.35}$$

or:

$$J_{conv_e} - J_{conv_w} = J_{dif_e} - J_{dif_w} \tag{3.36}$$

Rearranging:

$$J_e = J_w \tag{3.37}$$

where

$$J_e = J_{dif_e} + J_{conv_w}$$

$$J_w = J_{dif_e} + J_{conv_w}$$

Using central differencing into 3.37 gives:

$$D_e\,(n_E - n_C) + \vec{u}_e n_e = D_w\,(n_C - n_W) + \vec{u}_w n_w \tag{3.38}$$

The unknowns in equation 3.38 $n_e, n_w, \vec{u}_e, \vec{u}_w$ are obtained by simple linear interpolation.

Central differencing and linear interpolation applied to equation 3.38 leads to numerical instabilities 3.8 whenever $|P_e| > 2$, as showed in [45, 53]. In this case, the solution most of the time diverges rather than converging, producing oscillating or unrealistic solutions. This implies that a new method is needed for the discretization of the diffusion-convection equation.

Several methods are available for the general solution of the diffusion-convection equation, with the upwind method being the simplest to use [54]. In this approach, the unknowns n_e and n_w are not interpolated but approximated with the value at the upwind side. Another scheme, the so-called exponential scheme, was first proposed by Gummel and Scharfetter [55] in their semiconductor simulations. This method has been extensively used to discretize PDE's involving both first and second derivatives either in the semiconductor field [55] and in some plasma simulations [56–59]. Selberherr [60] derived similar expressions to discretize convective-diffusive flows based on exponentials following a more complete mathematical analysis. However, it is not clear whether or not these schemes are efficient enough to run in a workstation using a 3D mesh [53] due to the extensive number of calculations that are need involving exponentials. In an attempt to develop a more efficient scheme, Spalding [61] proposed a new model, the hybrid model, where the diffusion-convection equation is discretized avoiding the use of exponentials. The hybrid scheme is the base for the discretization of equation 3.8 in this thesis. This method has been proved to be efficient enough to solve the diffusion-convection problem [62, 63].

The hybrid scheme is well documented in literature [45, 53, 61–63]. The hybrid model splits the convection-diffusion equation in 2 cases, depending in

the value of $|P_e|$. When $|P_e| > 2$, the convective convective term is obtained using the upwind method whereas when $|P_e| < 2$ a linear interpolation scheme is used to get the unknowns values of n_e and n_w at the cell faces (the so-called central differencing, or the CDS scheme in [63]).

Using the hybrid scheme to discretize equation 3.8 yields:

$$a_P n_C = a_E n_E + a_W n_W + a_N n_N + a_S n_S + a_F n_F + a_B n_B \tag{3.39}$$

where

$$\begin{aligned}
a_E =& max\left[-\frac{\vec{u_x}}{\Delta x}, \left(\frac{D_e}{\Delta x^2} - \frac{\vec{u_x}}{2}\right), 0\right], a_W = max\left[\frac{\vec{u_x}}{\Delta x}, \left(\frac{D_w}{\Delta x^2} + \frac{\vec{u_x}}{2}\right), 0\right] \\
a_N =& max\left[-\frac{\vec{u_y}}{\Delta y}, \left(\frac{D_n}{\Delta y^2} - \frac{\vec{u_y}}{2}\right), 0\right], a_S = max\left[\frac{\vec{u_y}}{\Delta y}, \left(\frac{D_s}{\Delta y^2} + \frac{\vec{u_y}}{2}\right), 0\right] \\
a_F =& max\left[-\frac{\vec{u_z}}{\Delta z}, \left(\frac{D_f}{\Delta z^2} - \frac{\vec{u_z}}{2}\right), 0\right], a_B = max\left[\frac{\vec{u_z}}{\Delta z}, \left(\frac{D_b}{\Delta z^2} + \frac{\vec{u_z}}{2}\right), 0\right] \\
a_P =& a_W + a_E + a_N + a_S + a_F + a_B + \vec{u}_e + \vec{u}_n + \vec{u}_f - \vec{u}_w - \vec{u}_s - \vec{u}_b
\end{aligned} \tag{3.40}$$

with interface diffusivities linearly interpolated as in 3.32.

Equation 3.39 is the basic layout to solve diffusive plus convective transport in TS2. There are also other schemes mentioned in the literature to solve the diffusion-convection equation. One of them, the Power-law scheme, is the method recommended in [53] but its principal drawback is that it requires more operations per cell, being just slightly better than the hybrid scheme. Another method, the QUICK scheme [45], requires information about cells other than direct neighbors. This scheme is not suitable for SPUDII unless some other tools are added to the framework which is beyond the scope of this thesis.

3.3.1 Momentum

The momentum equation is solved following an approach similar to the one used in solving the diffusion-convection equation. The only difference is the inclusion of the pressure gradient.

There are still two important topics to be tackled in order to perform a complete simulation: boundary conditions and grid refinement. Next, both issues are addressed showing the strategies used to deal with them.

3.3.2 Boundary conditions

Equations 3.8 and 3.5 are mathematical abstractions that associate spatial and temporal variations of density and temperature in a specific medium. As stated before, they are just good approximations to the more complicated equations which are very difficult and inefficient to solve. The use of these equations is limited to several assumptions and simplifications which help to solve them numerically. One of the most important assumptions is the treatment of the boundary conditions.

For the simulation to provide a good estimation of the transport process, it is necessary to handle very carefully cells with boundary interfaces, i.e. walls, cathode, shutters, etc. A bad approximation for any interaction between the surrounding fluid and the surfaces will lead to an inaccurate or diverging solution.

To properly simulate diffusion and heat transfer, boundary conditions must be formulated at the interfaces. There are 3 basic kinds of boundary conditions: Dirichlet, Neumann and Robin conditions [64]. Mathematically, the

boundary condition is described by:

$$s = \alpha u + \beta \frac{\partial u}{\partial x} \tag{3.41}$$

It is said that there is a Dirichlet boundary condition whenever $\beta = 0$, while a Neumann condition is obtained when $\beta \neq 0$ and $\alpha = 0$. When both α and β are nonzero, a Robin condition is said to exist. There is also mentioned in the literature a fourth type of boundary condition [64] which is related to interactions between 2 solids, but this kind of analysis can be normally reduced to finally obtain a Robin boundary condition equation. This thesis only deals with Dirichlet and Neumann conditions at the obstructions.

In general terms, Dirichlet conditions are commonly associated with fixed values at the boundaries, i.e. a fixed value of temperature or density, whereas Neumann conditions are related to flux values at the interfaces. Robin boundary conditions can be found where interactions between gas and solid interface occur. SPUDII neglects the effect of sputtering gas inlet and outlets such that there is no external gas flow into the system.

SPUDII handles the obstructions in a special way. For SPUDII, there are no walls, neither cathodes or substrates: all the surfaces are treated as obstructions. These obstructions are set in the XML configuration file and in this way the software "knows" what they are and how they have to be treated.

The grid in TS2 only knows 3 kind of cells within the simulation region: inside cells, boundary cells and outside cells. This is showed in figure 3.4. A boundary cell is as well an inside cell. The basic routines that solve equations 3.8 and 3.5 sweep through the entire simulation region solving the transport equations.

In a typical sputter deposition process, there are 2 kinds of thermalized

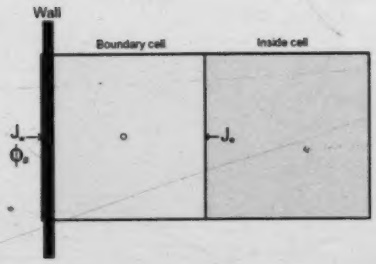

Figure 3.4: **Cell with an interface on it. This cell is defined as a boundary cell in SPUDII and should be treated with care. Depending in the species of gas, this cell behaves differently.**

neutral particles inside the chamber: the background gas and the sputtered particles. There are also metastable and excited particles which in turn are also neutral, but for the time being TS2 ignores them. There are of course some other deposition precesses where more than 2 neutrals species can be found (reactive sputtering, alloy deposition), but this problem will be investigated in a future work.

In general terms, walls react as substrates for sputtered materials (Dirichlet condition) while acting like mirrors for gas particles (Neumann condition). Taking a typical aluminum deposition process (depositing aluminum in an argon environment), the boundary conditions for the continuity equation for these 2 species are:

$$J_{Ar}\Big|_{wall} = 0\ (Neumann) \tag{3.42}$$

$$n_{Al}\Big|_{wall} = 0\ (Dirichlet) \tag{3.43}$$

or in terms of the sticking coefficient S:

$$S_{Ar} = 0$$
$$S_{Al} = 1 \tag{3.44}$$

It is also important to mention how energetic particles are treated in TS1 when colliding with obstructions. When an energetic neutral hits a wall one gets two different scenarios: if the particle being tracked is a target material, the particle is absorbed and sent to the histogram handler. However, if the particle is a background gas atom, it is assumed that the neutral is thermalized by the impact and hence it is mirror reflected with an energy equal to that of the wall. This treatment can be further improved if a special module is added to properly simulate interactions between energetic particles hitting solid obstructions, probably an inherited class of TARGSPUD.

In the case of the heat solver, TS2 assumes that the walls are kept at a constant temperature (normally ambient temperature) which leads to a Dirichlet condition. This constant temperature is preconfigured in the XML file at the beginning of the simulation. A Dirichlet boundary condition can be expressed as:

$$Temperature|_{wall} = T_{room} \tag{3.45}$$

Referring to figure 3.4, in a cell with a Dirichlet boundary condition, J_w is approximated via:

$$J_w \approx \kappa_C \left(\frac{T_C - T_{wall}}{\delta x/2} \right) \tag{3.46}$$

being J_e the same as for equation 3.30.

For T_{wall} several values have been proposed. The walls are not exactly at room temperature and heat conduction on the walls depends on the material

and thickness of the wall. Bogaerts *et al* [9] assumed a constant temperature of 300 K except for the cathode which is believed to warm up. If N_2 is used to cool the cathode they proposed a value of 300 K. In this paper, a study of the effect on the gas of varying cathode temperatures is reported. Turner *et al* [22] assumes a substrate and cathode temperatures of 350 K. They argued that substrates have been observed to reach temperatures $\sim 100K$ above room temperatures, making it necessary to include this effect in the boundary conditions. In a variant of the latter approach, the walls' temperature is left to rise to be equal to that of the neighboring cell. Bukowski [11] performed his simulations using a $T_{wall} = 300K$.

An alternative to the previous approach is to solve an equation which takes into consideration an effect that have been observed by several researchers. This effect is that the gas just next to the wall is not at the same temperature as the wall, especially at lower densities. This equation reads:

$$T_{g(wall)} = T_{wall} + \lambda(\nabla T_g)_{wall} \tag{3.47}$$

where:

$$\lambda = \frac{2-\alpha}{\alpha}\xi\xi_0\frac{T}{p\sigma} \tag{3.48}$$

and $\xi_0 = 0.6505 \times 10^{-23}$, α is a *thermal accommodation coefficient* and ξ is defined as:

$$\xi = \frac{c_p + \frac{5}{4}R}{c_p - \frac{1}{2}R} \tag{3.49}$$

where R is the universal gas constant. The numerical value of α depends on several factors and it is obtained by experimentation rather than theory because of the lack of information about this coefficient in literature[9]. This boundary treatment is used in [9, 33] and it is reported to work properly for

gas-solid interfaces. The ultimate goal of SPUDII is to have a module that simulates this interaction to have a better understanding of the whole process.

On the other hand, for Neumann boundary conditions, no approximation is required since one is interested in the flux at the cell face which is already known (assuming that all gas particles are reflected). Thus, according to equation 3.42, the flux at the wall is:

$$J_w = 0 \tag{3.50}$$

For the convective term, the non-slip stationary boundary condition is applied at the wall deriving in:

$$\mathbf{u}|_{\text{wall}} = 0 \tag{3.51}$$

Substituting equations 3.46, 3.50 into 3.29 gives the set of equations to be solved for cells that contain obstructions in them.

For the sake of simplicity, obstructions in the chamber are assumed to coincide with the cell faces. This approximation simplifies the analysis and implementation of the finite volume method. It could be argued that this approach of solving for boundary conditions is not a good approximation, especially if the cells are not small enough. Nevertheless, as soon as the cell becomes smaller, the real obstruction is closer to the cell boundary. This is a tradeoff of the model proposed and it is believed not to significantly affect the accuracy of the solution.

3.3.3 Refinement and grid transitions

Before exploring refinement, some new concepts regarding an octree have to be introduced. Referring to figure 3.5, a cell with size Δx=Δy=Δz=Δ is

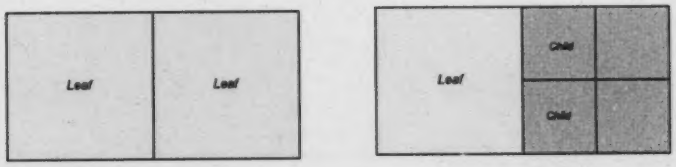

(a) leaf

(b) child

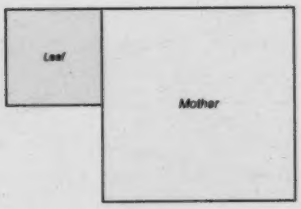

(c) mother

Figure 3.5: **Different interfaces found in a quadtree mesh. 3.5(a) shows a normal interface. 3.5(b) depicts a normal cell with a refined boundary and 3.5(c) shows a refined cell with a normal cell as boundary**

defined as a LEAF cell. The solver is always referred to be solving for a LEAF cell. A CHILD cell is that neighbor cell eight times smaller than the LEAF cell (as a result of local refinement of a LEAF cell) and a MOTHER cell is that neighbor cell eight times bigger than the LEAF cell (only one level of refinement is assumed to be performed).

When the solver finds an interface where the neighboring cell is not equal in size to the LEAF cell itself, discretization of the transport equations requires special treatment. Central differencing approximations cannot be directly used since there is no information regarding the value of the variables at those points located not in the center of the control volume (ghost points). To properly approximate the flux between two control volumes using the finite volume

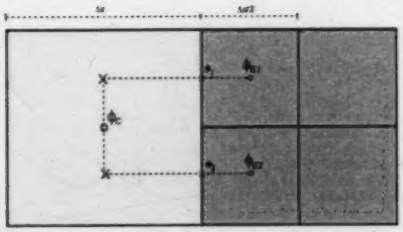

Figure 3.6: **Lack of information about points X. These points are needed in order to discretize equation 3.5 using finite volume method. Linear interpolation is required to obtained the values.**

method, information about the local values at ghost points is needed. This problem is depicted in figure 3.6. Note that there is no stored information whatsoever about density or temperature at ghost points.

This problem is solved in different ways. Martin *et al* [36] and Popinet [37] used quadratic interpolation to obtain ghost values needed to approximate the flux at the interfaces. Borthwick *et al* [34] performed linear interpolation to approximate the flux between cells. De Marsily [65] used a scheme based in Taylor expansions over a point at the interface of interest. In [37] it is argued that Quadratic interpolation is more accurate since, for central finite difference approximations to conserve second order accuracy, a second order interpolation scheme is required. A major drawback of using a second order interpolation schemes in TS2 is that the set of linear equations obtained after applying interpolation is very difficult and expensive to solve using SPUDII tools. These complications come from the fact that values which are not easily obtained using standard functions in SPUDII are needed. For this reason, an approach using linear interpolation similar to the one derived in [34] is used to obtain the required values.

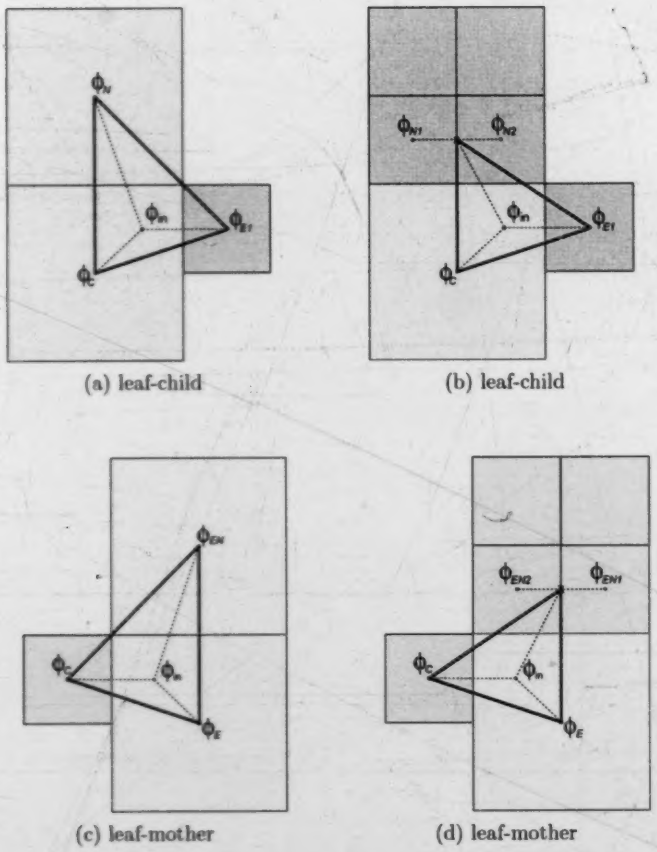

Figure 3.7: **Linear interpolation for a quadtree mesh. Values of ϕ_{in} are obtained by linear triangular interpolation. TS2 uses an extension to 3D via tetrahedral interpolation.**

A tetrahedral interpolation model is proposed to obtain the required values. Using an extension to 3D of the scheme showed in figure 3.7, and assuming only one level of refinement, 3 cases can be identified: only one face refined, two faces refined and 3 faces refined. It is assumed that the software only allows a maximum of 3 refined faces per cell. Assuming all cells are cubic, a treatment similar to that of section 3.3 leads to the next set of equations:
For case 1, assuming the N face is refined:

$$T_C = \frac{5}{34}T_E + \frac{5}{34}T_W + \frac{5}{34}T_F + \frac{5}{34}T_B + \frac{3}{16}T_S + \frac{1}{17}T_{N_R}$$

For case 2, assuming the N and F faces are refined:

$$T_C = \frac{6}{47}T_E + \frac{6}{47}T_W + \frac{15}{94}T_B + \frac{15}{94}T_S + \frac{10}{47}T_{N_R} + \frac{10}{47}T_{F_R}$$

For case 3, assuming the N, F and E faces are refined:

$$T_C = \frac{4}{21}T_{E_R} + \frac{1}{7}T_W + \frac{4}{21}T_{F_R} + \frac{1}{7}T_B + \frac{2}{21}T_S + \frac{1}{7}T_{N_R} \qquad (3.52)$$

where

$$T_{N_R} = \frac{1}{4}\left(T_{N1} + T_{N2} + T_{N3} + T_{N4}\right)$$
$$T_{E_R} = \frac{1}{4}\left(T_{E1} + T_{E2} + T_{E3} + T_{E4}\right)$$
$$T_{F_R} = \frac{1}{4}\left(T_{F1} + T_{F2} + T_{F3} + T_{F4}\right)$$

In equation 3.52, the values T_{Ni} are the 4 neighbor cells when the N face is refined.

Equations 3.52 are the basic equations used to solve for a oct-tree mesh in SPUDII.

3.4 Solution of linear equations

Once the set of algebraic equations has been obtained, a proper numerical method must be applied to solve it. Given the weak nonlinearity of equations 3.5 and 3.8, direct methods are not recommended [45]. Further more, it is desired to avoid the use of direct methods when the number of points to be solved for exceeds 10000 [66]. A simple strategy to solve non-linear equations with a big number of points is to use an iterative procedure [45].

Among iterative methods, Gauss-Seidel is the most appropriate choice for TS2 since SPUDII has special tools to sweep through the entire domain using Newton's method as required in this method. Furthermore, there is no need to store any matrix or to solve any large system of equations.

Even though there are some other methods available for non-linear elliptic equations which are argued to be more efficient [67], it is not clear that they are actually more efficient for the solution of the convection-diffusion equation in non-uniform grids. For this reason, a non-linear Gauss-Seidel algorithm is applied in the present thesis to take advantage of the resemblance between both equations (diffusion-convection and heat transport). Both solvers share several functions which, in terms of efficiency, is an attractive characteristic to be exploited.

Gauss-Seidel was introduced in subsection 3.3 and its application to diffusive plus convective problems is straightforward. Frequently, the convergence rate can be further improved if a technique known as successive overrelaxation (SOR) is applied. SOR is commonly used to accelerate the rate of convergence of the Gauss-Seidel iteration scheme.

Overrelaxation is an interpolation procedure. The idea behind overrelax-

ation is to obtain an intermediate value of n_c called $n_c^{\overline{k+1}}$ between iterations using Gauss-Seidel as:

$$n_c^{\overline{k+1}} = \frac{1}{6}\left(T_E^k + T_W^{k+1} + T_N^k + T_S^{k+1} + T_F^k + T_B^{k+1}\right) \tag{3.53}$$

where n_c^k is the value obtained in the previous iteration. Then, one uses the $n_c^{\overline{k+1}}$ to extrapolate a value for n_c^{k+1} using:

$$n_c^{k+1} = n_c^k + \omega\left(n_c^{\overline{k+1}} - n_c^k\right) \tag{3.54}$$

where ω is the *overelaxation index*. Equation 3.54 is known as the Successive Overrelaxation (SOR) method. The optimum value of ω depends on the size of the cell and it is obtained heuristically.

The algorithm depicted in 3.54 is then applied to all the cells in the domain and a final value for n_c is obtained. To determine convergence, a local truncation error is monitored in each cell until its value lies below a maximum value e. The local truncation error is calculated using expression 3.55. The numerical value of e can be easily changed when compiling the code or if necessary at run time through the XML file. A low value of e will produce a more accurate solution, with the obvious expense of additional computational time. The expression to calculate e is:

$$e = \frac{\left|n_c^{k+1} - n_c^k\right|}{max\left|n_c^k\right|} \tag{3.55}$$

As a final remark, it is necessary to comment that the rate of convergence and the use of non-linear SOR to solve both equations 3.8 and 3.5 strongly depends on a good initial guess. The closer the initial iteration is to the final result, the higher the rate of convergence and the faster the code converges. As a consequence, a good estimation of the solution is required to have a stable and efficient code.

3.4.1 Thermalization threshold

An important value related to TS2 is the value at which particles are considered thermalized. Ideally, particles should be followed until they reach thermal energies and a final distribution is obtained. This approach is very inefficient to perform as was explained before. Most of the work done so far involving thermalization is focused rather on obtaining distributions of thermalized particles while neglecting their transport once they have reached thermal energies. Neglecting this transport may underestimate the effect of thermalized particles in the film properties. It is assumed that thermalization is a faster process than diffusion so it can be presumed that thermalization has been finished when diffusion starts.

The concept of the thermalization threshold was introduced at the beginning of the chapter. It is clear to conclude that a large value for the thermalization threshold increases the population of thermalized particles which in turn increases the power deposited in the gas using this proposed model. On the other hand, a small value of the thermalization threshold would cause that the power input into the gas to be small.

In treating thermalization and energetic transport, Serikov and Nanbu [33] have proposed the use of a threshold value of $9E_{th}$, where $E_{th} = \frac{3}{2}kT$. In their work, they made a brief analysis of the effect of choosing different values for the thermalization threshold on the power deposition into the gas. They concluded that an optimum value of $9E_{th}$ is appropriate for this threshold (actually, they proposed a value of $3v_{th}$, where v_{th} is the mean thermal velocity). Despite the fact that the analysis performed by these researchers only refers to Ar^+-Ar collisions, this expression can be used as an initial approximation to the case of Ar_{fast}-Ar collisions. Bogaerts *et al* [9] also used $9E_{th}$ for their calculations.

In another work not involving magnetron simulations, Bogaerts *et al* [32] used a fixed energy threshold (0.06 eV) to differentiate fast atoms from thermal ones. The energy threshold in TS2 can be configured in the XML file at run time to investigate the effect of different thresholds in the final distribution and temperature of the background gas.

3.5 Algorithm

3.5.1 TS2 Algorithm

The algorithm chosen to solve the transport of thermalized neutrals is depicted in figure 3.8. An iterative scheme was chosen for reasons already explained. Convergence is defined when the results of 2 successive simulations differ by less than a predetermined value.

Some other schemes were tested, however, the latter algorithm showed to be the bests overall. Special care was taken in solving the coupled continuity-momentum equations to avoid divergence and numerical instability. This special handling was related to the way on which this coupled system was solved. The continuity solver was underrelaxad instead of overrelaxed as suggested in [45] to handle the strong coupling of the momentum and continuity solver.

3.5.2 THERMSPUD Algorithm

TS1 and TS2 works iteratively until the convergence criteria is reached. The convergence criteria for this case is actually the same as for TS2:

$$T_{k+1} \approx T_k \leq 0.001 Max|T_k| \tag{3.56}$$

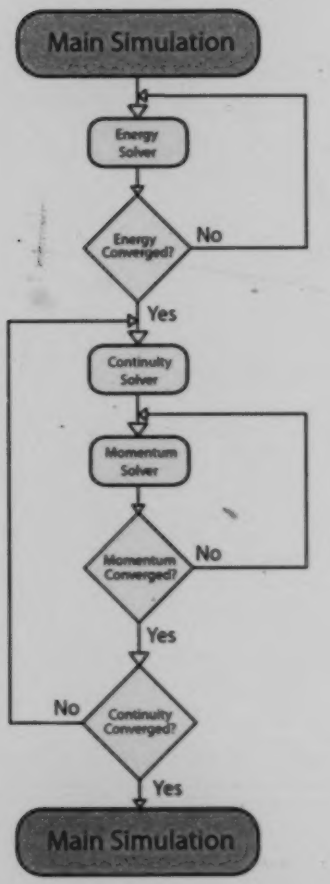

Figure 3.8: **Algorithm for TS2. Given the assumption of no convective heat transfer, the heat equation is purely conductive dominated. The heat and momentum solver were overrelaxed, while the continuity solver was underlexated due to the strong coupling between the continuity and the momentum equation.**

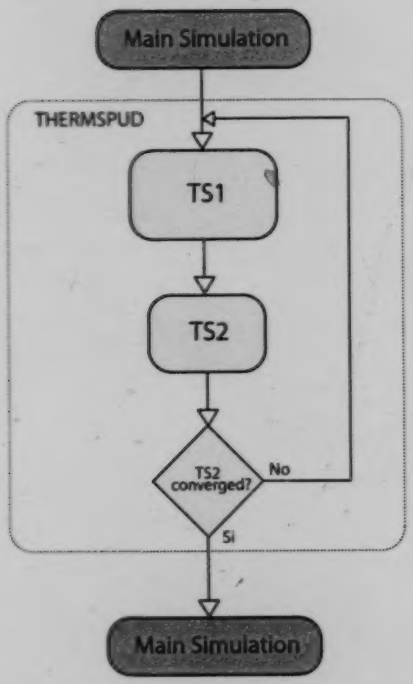

Figure 3.9: **Algorithm for a TS1 and TS2 simulation. Every time a full iteration is performed, the new density and temperature profiles are inputs for a new TS1 iteration. This procedure is followed until changes in density and temperature in consecutive global iterations are small.**

and

$$n_{k+1} \approx n_k \leq 0.001 Max|n_k| \tag{3.57}$$

The algorithm for a THERMSPUD simulation is shown in figure 3.9. THERMSPUD1 solver had to be slightly modified to be properly coupled with TS2.

Chapter 4

Results

4.0.3 Chamber and system configuration

Figure 4.1 shows the chamber configuration used in the study presented in this thesis. This chamber is representative of a typical magnetron chamber.

A set of numerical experiments are reported on the next sections to show the performance of TS2 for simulating a deposition process. The study was conducted with the following simulation parameters:

- Chamber: 0.3 x 0.3 x 0.3 m.
- Base pressure: 1, 5, 10, 15 and 20 mTorr
- Target to substrate distance: 10.1 cm
- Sputter gas: argon
- Target material: aluminum, copper
- Room temperature: 300 K
- Cathode potential: -300 V
- Erosion profile: experimentally measured aluminum target (see figure 2.5)
- Walls (other than cathode) potential: grounded

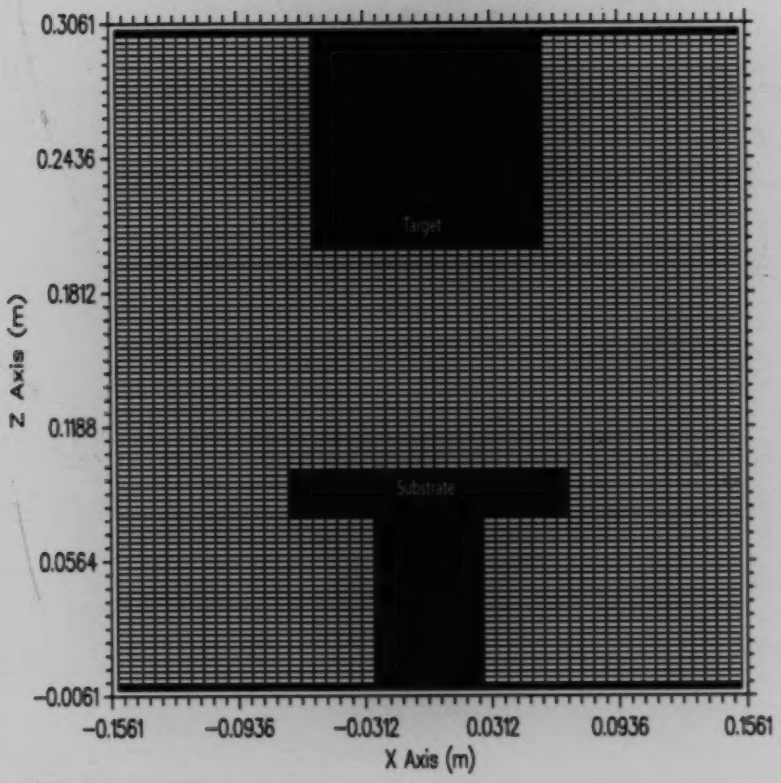

Figure 4.1: **Chamber configuration for simulating aluminum deposition in a magnetron sputtering system. The substrate and target are located 10 and 20 cm respectively above the base of the chamber. The base is set to be the zero reference in the z axis.**

The walls of the apparatus were assumed to be at room temperature. The target was also assumed to be at room temperature (given an ideal cooling system).

Two important parameters needed for this numerical investigation are those values related with the target material: the total yield and the neutral reflection coefficient. These values where obtained from [68] and input into the simulation in the XML file.

All simulations were performed on Intel Pentium IV @ 1.7 GHz machines with 256 MB of RAM running linux. It took approximately 8 hours for TS1 to run and 6 hours for TS2 to converge. The mean number of global iterations during the experiments was 4 total iterations.

4.0.4 External modules

As part of the simulation requirements, the ParticleGenerator object was updated with a realistic erosion profile. The erosion profile used in this study was obtained from a real aluminum target (see figure 2.5) and entered in the simulation as a text file. The ParticleGenerator object handles this text file. Figure 4.2 depicts a plot of the text file used as the erosion profile in this work.

As for angular and energy distributions, the ParticleGenerator object used an existing model [68] to obtain the angular and energy distributions of sputtered particles. The reader is referred to previous reports regarding this topic [8, 69].

Figure 4.3 shows the XML interface used to create a configuration file for a user-defined simulation. Note how all simulation parameters are input in a single XML file.

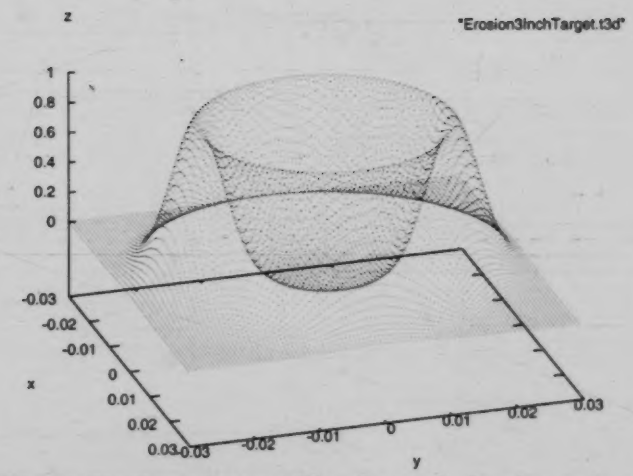

Figure 4.2: **Normalized erosion profile of a real aluminum target in a magnetron sputter deposition system.**

4.1 Simulation results

The numerical results reported in this thesis were obtained at 5 different pressures. At each pressure, a set of 5 simulations at different powers was performed. It has to be noted that the results presented were taken along the z axis at the center of the erosion profile. Emphasis has to be made in noting that, as showed in figure 4.1, the substrate and target are located at 10 and 20 cm above the base of the chamber, respectively.

Temperature, gas rarefaction and diffusive flux of sputtered atoms are reported as functions of power and pressure. The target to substrate distance was kept constant for most of the results reported.

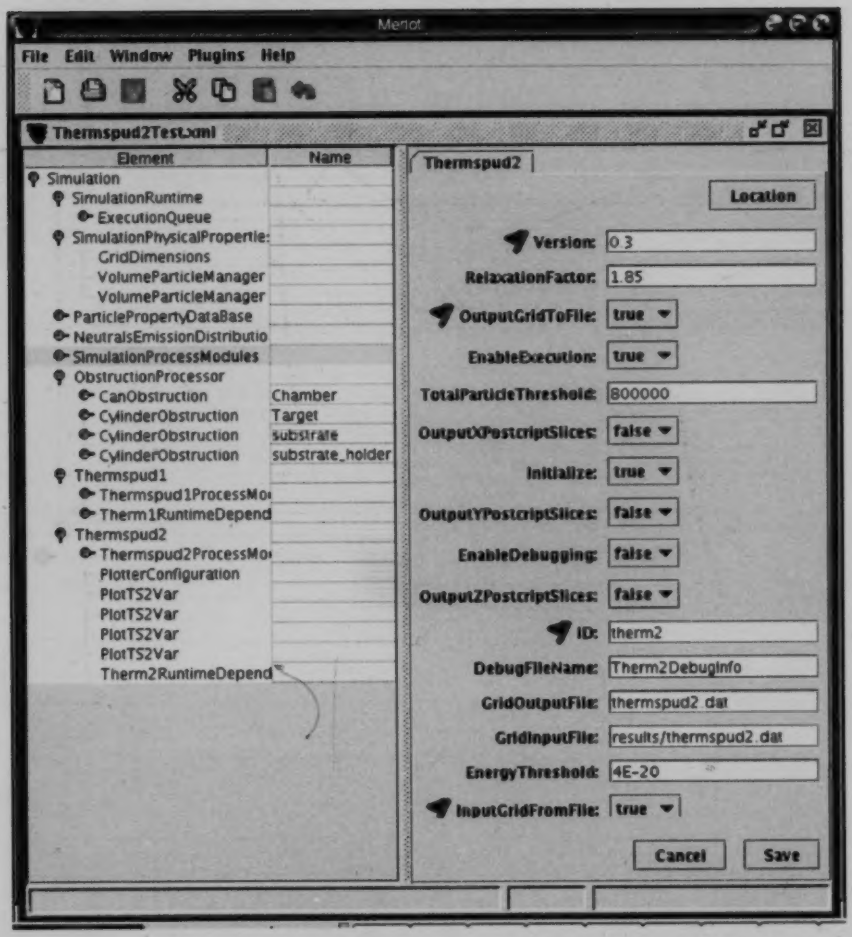

Figure 4.3: **XML configuration file for a SPUDII simulation. In this example, the simulation is configured so TS1 and TS2 have been added to the simulation object. The configuration file was edited using the open source Merlot XML editor.**

4.1.1 Temperature profiles

In figure 4.4, gas temperature is plotted in the z direction. Values were taken at the center of the target along the z axis. As would be expected, the general trend in the spatial profile indicates an increase in the maximum temperature with power. An increase in pressure shifts the location of the temperature peaks closer to the target, as the ejected energetic particles lose their energy more quickly.

Figure 4.5 depicts temperature profiles for five different powers. Peak gas temperature increases with pressure at all power levels considered.

To understand the effect of pressure and power, maximum temperatures as function of power and pressure are plotted in figures 4.7 and 4.6. One can see the linear dependence of T_{max} with respect to power, whereas with respect to pressure it is nonlinear. A maximum saturation temperature can be observed for different pressures. The value at which all the individual curves in figure 4.7 tend to saturate depends on several factors such as substrate distance, target radius, chamber configuration, sputtering gas, etc. Values reported here are only valid for this chamber configuration.

As for experimental validation, it is difficult to compare these results with experimental measurements due to the complexity of the processes and because measuring temperatures in a near vacuum is quite difficult. However, figure 4.8 compares results of THERMSPUD with corresponding values reported in [16] to see the performance of THERMSPUD module. Overall, THERMSPUD is capturing the correct trend and magnitude of the heating. Variations may be due to parameters mismatch, chamber heating, gas flow and experimental error. The overall agreement suggests that that energy is indeed mostly transported by conduction. Convective transport and gas flow appear to be less

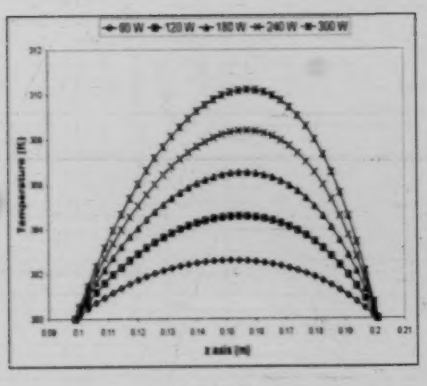

(a) 1 mTorr

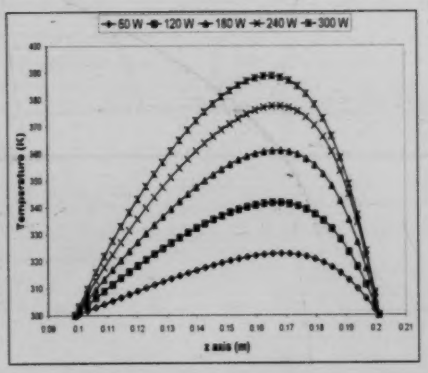

(b) 5 mTorr

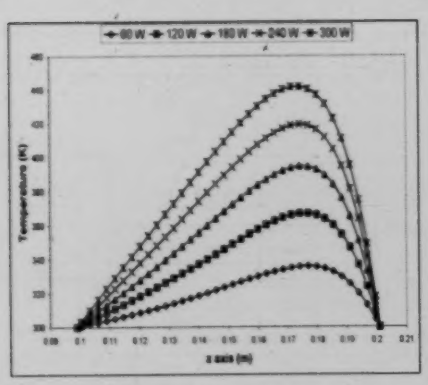

(c) 10 mTorr

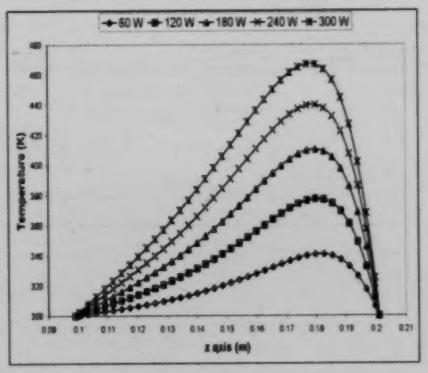

(d) 15 mTorr

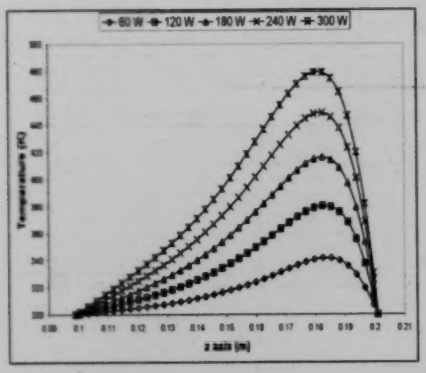

(e) 20 mTorr

Figure 4.4: **Power effects on gas temperature for 5 different pressures. According to figure 4.1 the target is 20 cm above the base of the chamber while the substrate is located at 10 cm from the base.**

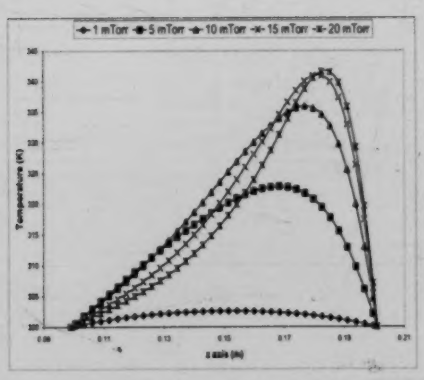

(a) 60 W

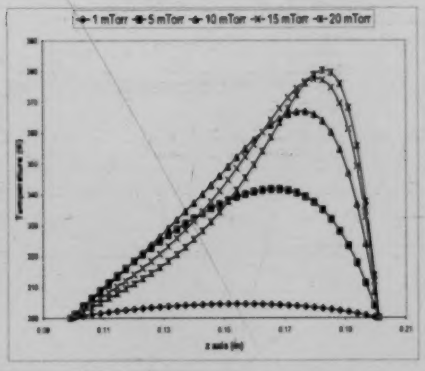

(b) 120 W

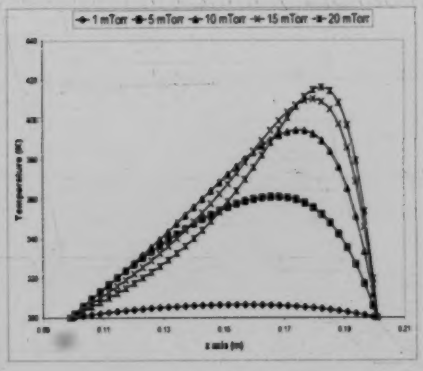

(c) 180 W

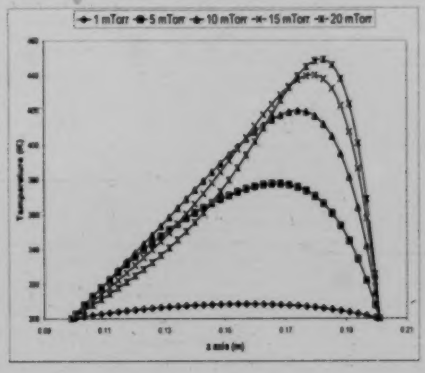

(d) 240 W

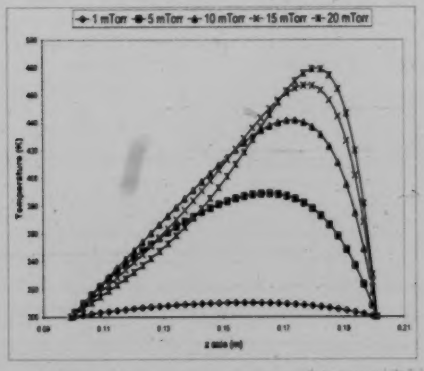

(e) 300 W

Figure 4.5: **Pressure effects on gas temperature for 5 different powers.**

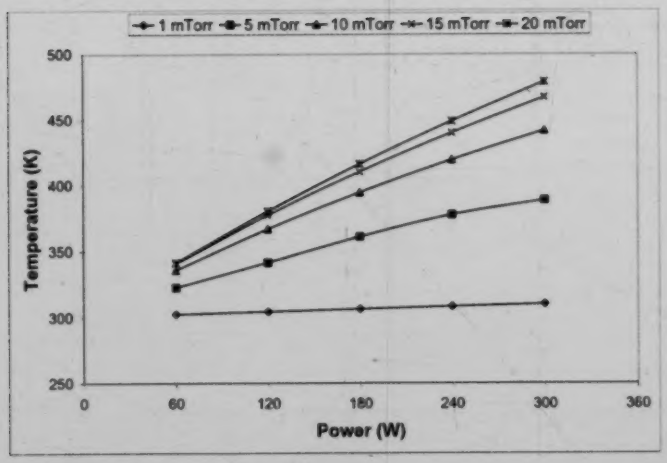

Figure 4.6: **Maximum temperatures as function of power at various pressures.**

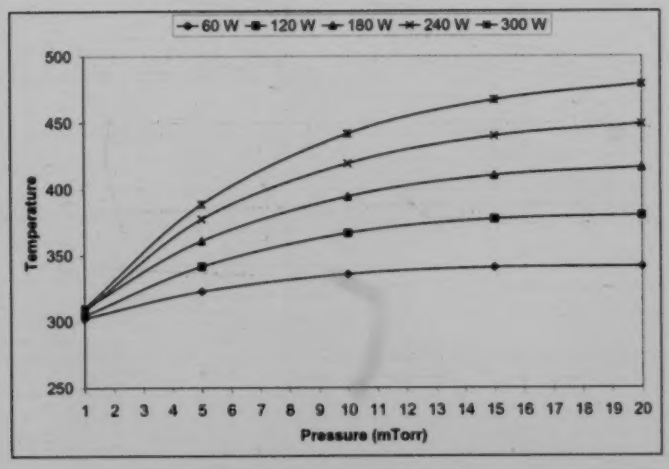

Figure 4.7: **Maximum temperatures as a function of pressure at various powers.**

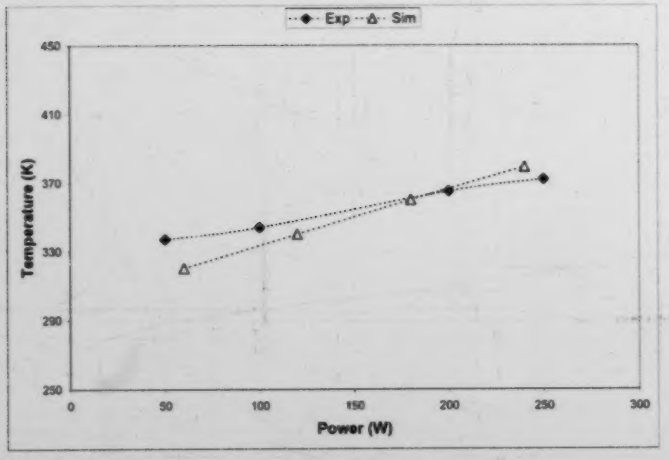

Figure 4.8: **Comparison between simulated temperatures and values reported in [16]. Experimental data is for aluminum, 8 cm substrate separation and 10 mTorr.**

important, although further confirmation of this is necessary.

As commented earlier, the constant wall temperature boundary condition is a limitation of the solver. The implementation of a chamber heating module is beyond the scope of this project. However, it is possible to set a different temperature for each wall which in some cases could overcome the lack of a chamber heating module. The problem with this approach is that a specific temperature for each deposition variables is necessary, and most of the times these values are not a known a priori. Figure 4.9 shows the temperature profiles for two simulations having different target temperatures. It is clear that the effect of a hotter target influence the heat flux at the substrate. Also, the transport of energetic neutrals is affected but it is believed that the influence is not significant. The overall effect should be investigated in a future work where a chamber heating module is incorporated into the SPUDII project.

During the deposition of copper, the background gas gets hotter than for

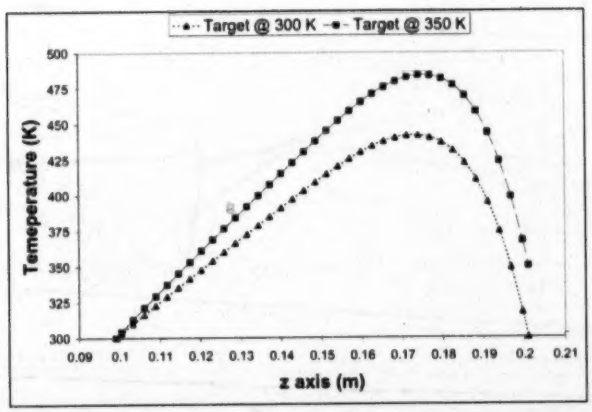

Figure 4.9: **Simulation results for two different target temperatures. Results are obtained assuming a target temperature of 350 K during deposition. Simulation is for aluminun deposition at 10 mTorr and 300 W.**

aluminum deposition, as figure 4.10 shows. This increment in temperatures could be explained by two factors. First, copper has a higher sputtering yield than aluminum. Hence, more material is sputtered given a particular power level. Second, the heat transfer mechanism is more efficient for copper given the higher mass of copper with respect to aluminum, depositing more energy into the gas per collision. Remember that, in a two-body elastic collision, the closer the masses the higher the energy transfer function which means a more efficient energy transfer process [39].

Finally, figures 4.11 and 4.12 shows a grey scale and a 3D plot of gas temperature where one can see the target and substrate shadowing effect. These plots are shown to give an idea of the kind of information one can gather from THERMSPUD.

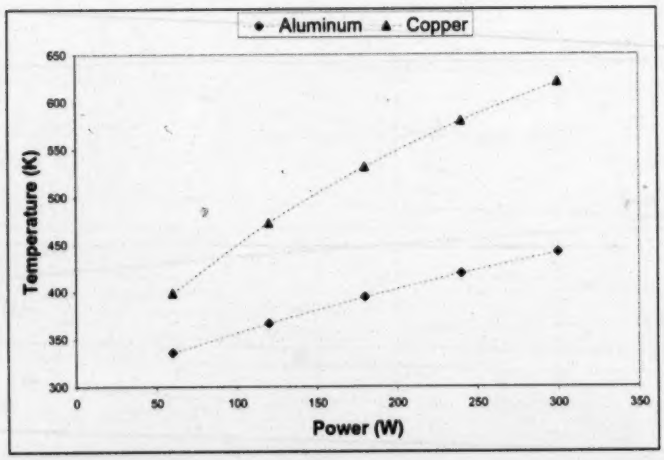

Figure 4.10: **Simulation results for aluminum and copper deposition. Note the higher temperatures for copper deposition when compared to aluminum.**

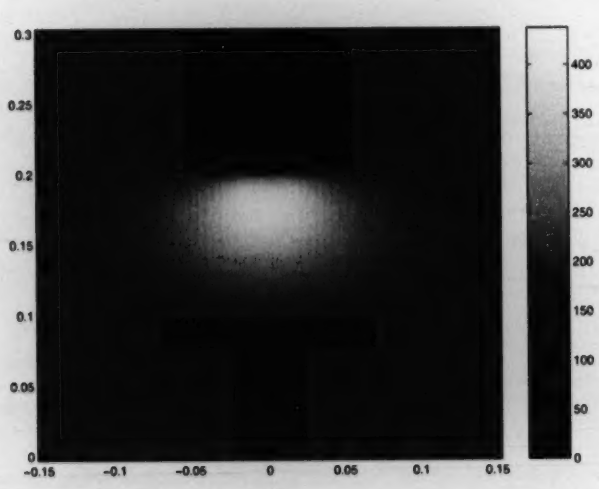

Figure 4.11: **Gray scale plot of temperature for aluminum deposition. Data is for 10 mTorr at 240W.**

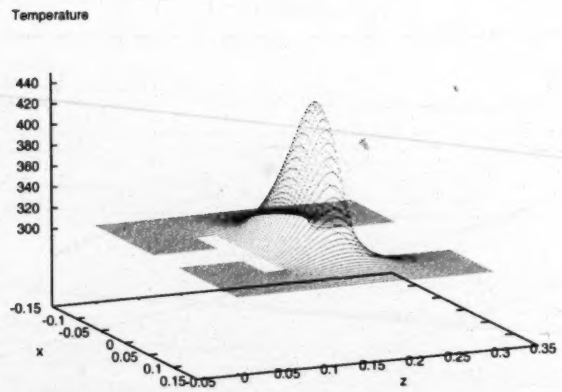

Figure 4.12: **3D temperature profile for aluminum deposition. All the obstructions in the chamber have a constant temperature. Data is for 10 mTorr at 240W.**

4.1.2 Density profiles

Argon

The rarefaction of Ar for different pressures and powers is showed in figure 4.13. From this figure one can see that the rarefaction effect depends on pressure and power. The gas gets hotter as these parameters are increased therefore there is more depletion in the zone close to the target. Note how for low pressures and powers there is not significantly rarefaction ($\approx 5\%$ for 5 mTorr at 60 W and $\approx 12\%$ for 20 mTorr at 60 W) but it is as much as 40% for 20 mTorr at 300W.

Figure 4.14 plots the maximum argon depletion as function of power for different pressures and figure 4.15 plots maximum depletion as function of pressure. Note how for the maximum depletion there is a nonlinear dependence in pressure. For a same power level in figure 4.15, one can note that the change

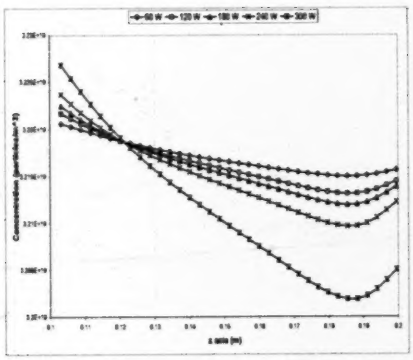

(a) 1 mTorr

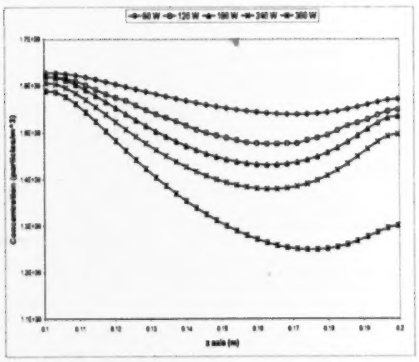

(b) 5 mTorr

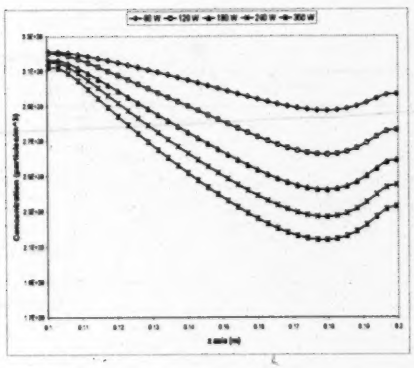

(c) 10 mTorr

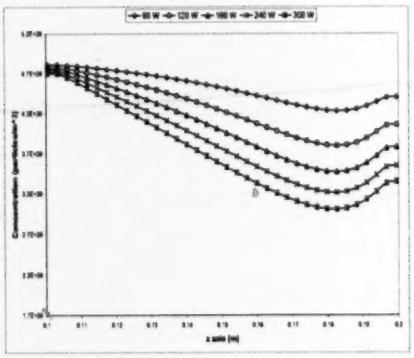

(d) 15 mTorr

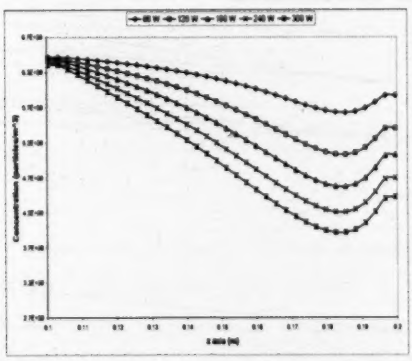

(e) 20 mTorr

Figure 4.13: **Power effects on Ar for 5 different pressures.**

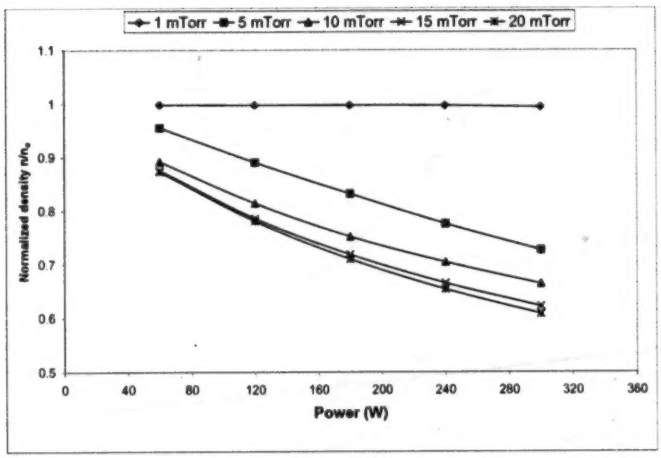

Figure 4.14: **Maximum density reduction as function of power for aluminum deposition.**

in concentration is nonlinear as pressure is increased converging to a final value. In contrast, for a given pressure in figure 4.14 and for increasing power, the maximum change in concentration follows a linear dependence. Further more, they have a very similar slope above 5 mTorr. The relative change in concentration is more dramatic at low pressures but this may be because of the uncertainty about the continuum solver in the low pressure regime for this configuration.

Results for rarefaction from TS2 are also compared to experimental measurements. First, in figure 4.16 the normalized gas density is plotted as a function of the discharge current. Rossnagel [15] found an experimental expression for the normalized gas concentration as a function of several parameters. These variables depend on several factors such as geometry of the apparatus, wall temperature and a factor that approximates the number of collisions for the atom to lose almost all its initial energy. Even though both exponents differ (Rossnagel found that this expression should be proportional to $I^{-0.5}$

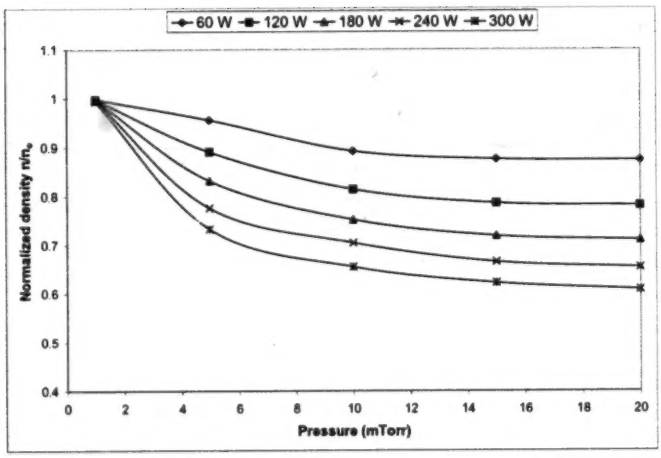

Figure 4.15: **Maximum density reduction as function of pressure for aluminum deposition.**

in the limit of high current and high pressure), the general trend found by Rossnagel can be observed. There is reduced agreements at low current as the empirical relation diverges in the limit of low pressure and current. Overall, however, this suggests that power law scaling could be valid for this specific configuration. It may be possible that the exponent for the power law found by Rossnagel could be overestimated due to the simplifications of his model, his chamber configuration and the uncertainty in the measurement technique.

To compare the minimum normalized concentration with experimental results, a similar plot to figure 4.8 is shown in figure 4.17. Data is again obtained from [16]. Note the bigger depletion found in simulation when compared to experiments. The disagreement could be due to the uncertainty in the measurement technique and also to the fact that, even though convective mass transfer is included when solving mass transport, it is assumed that there is no *total* gas flow from the outside. Having a *static* system implies that the rarefaction effect is not affected by the flow rate and pumping speed. This

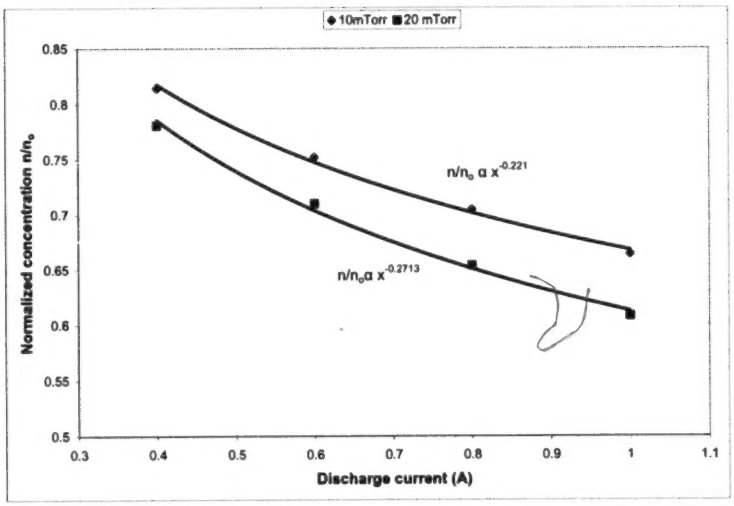

Figure 4.16: **Argon depletion as function of target current. The normalized concentration follows an empirical I^{-x} law previously found by Rossnagel [15].**

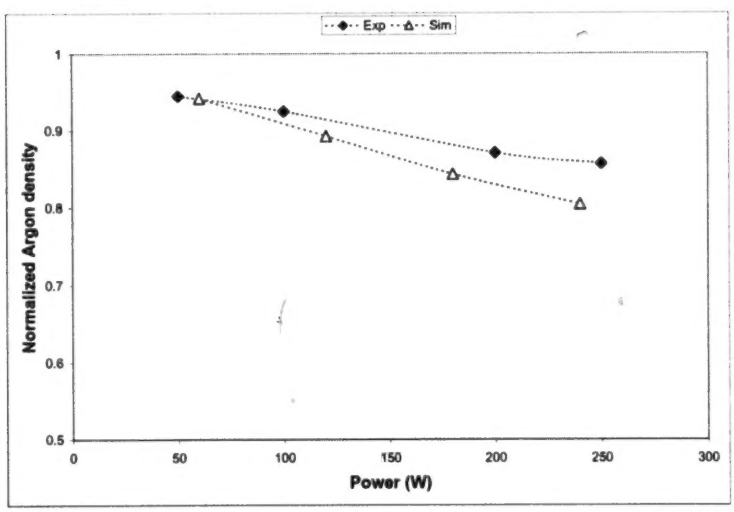

Figure 4.17: **Experimental normalized concentration vs simulated results.**

figure may imply that the level of gas depletion can be affected by the flow coming from the inlet and going to the pump. There is, however, also another important issue that may influence the results. The hot plasma may also affect the background density distribution, not decreasing rarefaction but accentuating the effect. It has been reported a significant contribution from the plasma in the rarefaction effect for high density plasma applications [70, 71]. This effect has been neglected and requires more investigation. In the SPUDII project, however, there is still some issues to tackle regarding PLASPUD and this module could not be included in the present study. It has been assumed in this thesis that it is possible to neglect these effects for the kind of results this thesis is focused on, as discussed earlier.

Another important observation from the results obtained in THERMSPUD, is the fact that ignoring the momentum solver in TS2 does not produce as much rarefaction as reported in literature. It is important that one does not neglect the momentum being deposited into the gas as a byproduct of the high energy transport. Whether or not to solve the momentum equation becomes critical depending on the power and the pressure regime. Figure 4.18 compares two simulations where the effect of solving or not the momentum equation is shown. This result may suggest that one significantly underestimates the amount of rarefaction when the momentum solver is omitted.

For comparison with Cu, figure 4.19 compares the rarefaction of the background gas for depositing 2 different materials. Cu deposition, which was found to have a higher gas temperature when compared with Al deposition, shows more neutral depletion between the target and substrate.

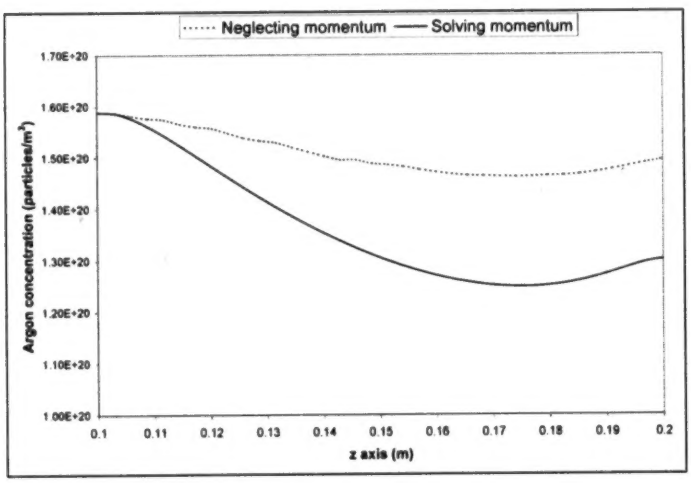

Figure 4.18: **Effect of neglecting the momentum equation in TS2. When momentum is omitted one does not observe the level of rarefaction reported in literature. Data is for 5 mTorr and 300 W.**

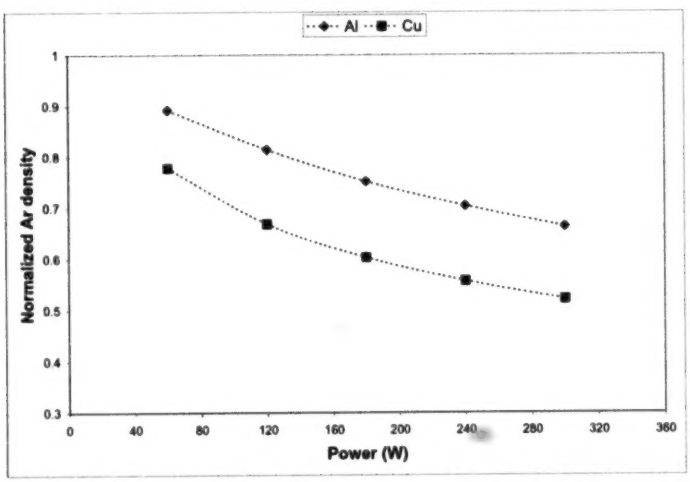

Figure 4.19: **Normalized Ar density for depositing Al and Cu as function of power. Data is for 10 mTorr.**

Aluminum

For the sputtered particles it is also possible to obtain a density distribution of the thermalized sputtered particles. Emphasis has to be made on the fact that these values are not total densities, but just the thermalized population. For a total sputtered particle distribution, TS1 code should be updated to gather particle distributions for the energetic sputtered particles. Figure 4.20 shows the power effect of varying power for different pressures.

An important result can be obtained by comparing the respective contribution of energetic and thermalized components of the total flux hitting the substrate. Assuming a unitary sticking coefficient, one can approximate the diffusive thermalized flux using Fick's law. A simple modification in TS1 also allows the software to obtain a flux of energetic particles hitting the target (also assuming unitary sticking coefficient). Figure 4.22 depicts the contributions of diffusive and energetic flux to the total flux impinging the substrate. For the distances considered, above 5 mTorr, the flux is almost totally of thermalized particles.

4.1.3 Iterative effects on TS2 results

As TS1 and TS2 iterate, the results obtained from TS2 vary depending on the system configuration. In figure 4.23, 2 different results of TS2 are plotted for 3 different power using the iterative scheme of figure 3.9 for an aluminum deposition process. It is interesting to note that at low power, the results of the first TS1 iteration are similar to the last one. This is logical since there is not much rarefaction as the temperatures are low. On the other hand, at high pressures, one can see a significant reduction in the maximum temperature after iteration ($\approx$ 30 degrees reduction).

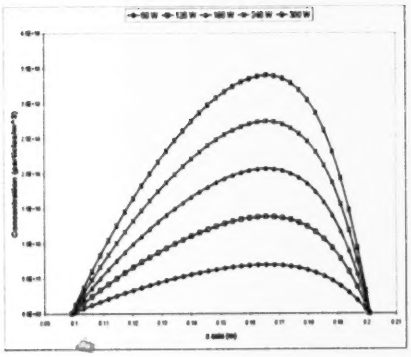

(a) 1 mTorr

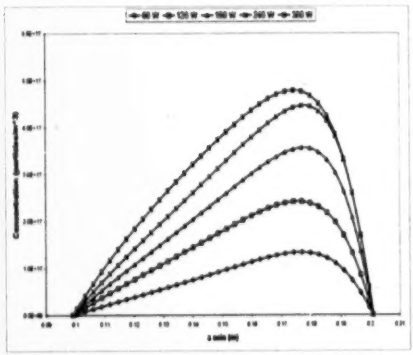

(b) 5 mTorr

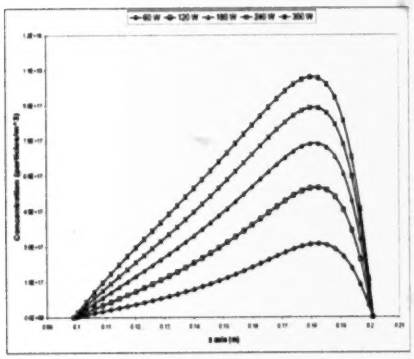

(c) 10 mTorr

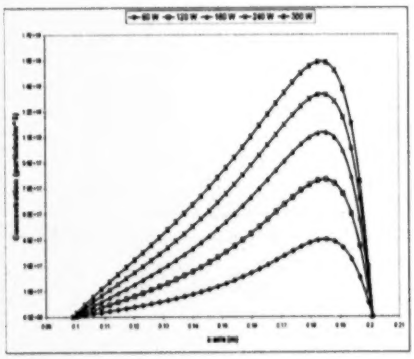

(d) 15 mTorr

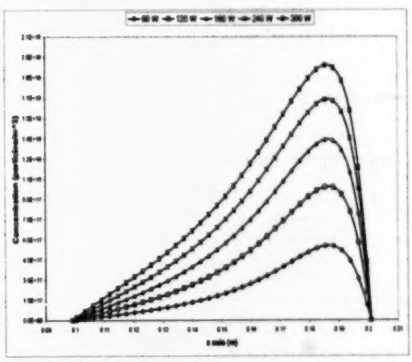

(e) 20 mTorr

Figure 4.20: **Power effects on thermalized aluminum concentration for 5 different pressures.**

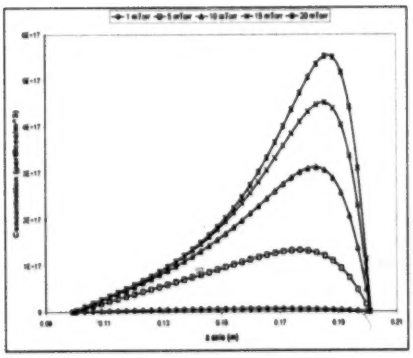

(a) 60 W

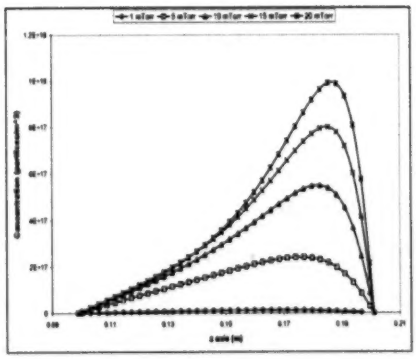

(b) 120 W

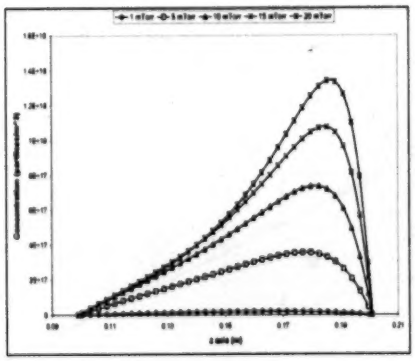

(c) 180 W

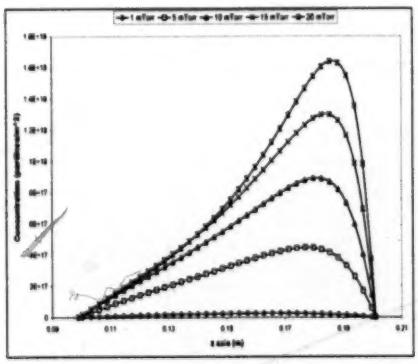

(d) 240 W

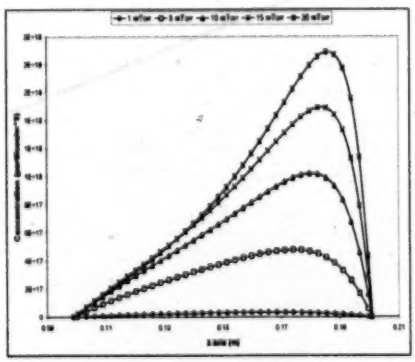

(e) 300 W

Figure 4.21: **Pressure effects on aluminum concentration for 5 different powers.**

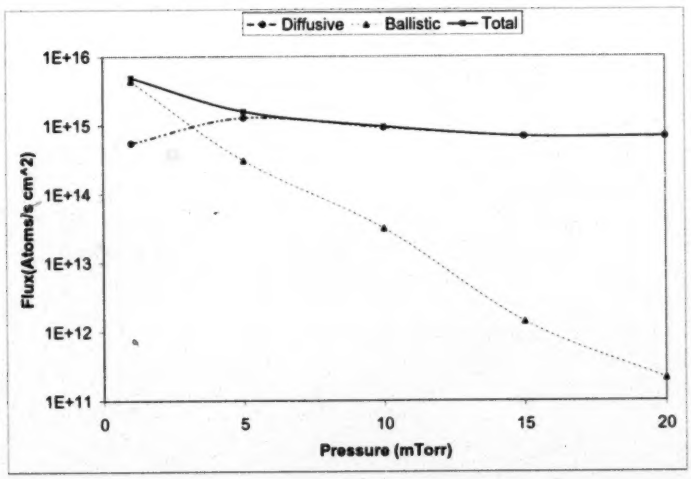

Figure 4.22: **Contribution of diffusive and energetic flux of sputtered particles to total deposition. The diffusive flux dominates the deposition at the substrate for pressures above 5 mTorr for this specific configuration.**

For copper, the differences are even more significant. Figure 4.24 shows the same data as figure 4.23 but for sputtering copper. As this figure indicates, the nonuniform temperature and density field obtained in TS2 affects the results of TS1 in a significant manner. This implies that for copper, the coupling between TS1 and TS2 becomes more important. This could explain the higher temperatures found in previous works [22]. Note, however, that results from reference [22] were for 500 W using a point source (high power density).

4.1.4 Target to substrate distance, effects on TS2

Figures 4.25 and 4.26 shows the effect of increasing the target to substrate distance. The target to substrate distance was increased to 15 cm and a similar numerical simulation was performed to be compared to data for 10 cm.

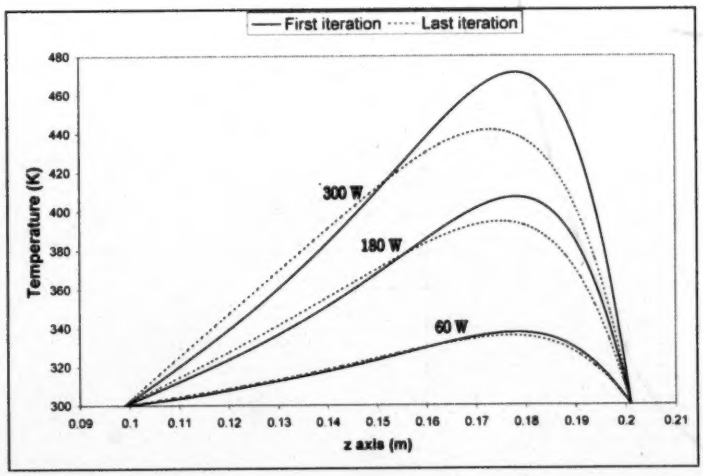

Figure 4.23: **Effect of iteration between TS1 and TS2 for aluminum deposition. Shown are the temperature profiles after one iteration and after final convergence between the two modules. Data is for 10 mTorr.**

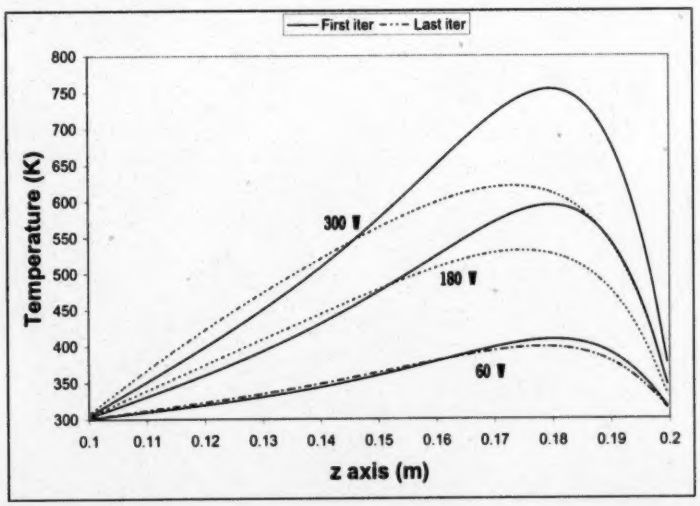

Figure 4.24: **Effect of iteration between TS1 and TS2 for copper deposition. Note how for high power the first iteration gives a higher temperature than the final converged data. Data is for 10 mTorr.**

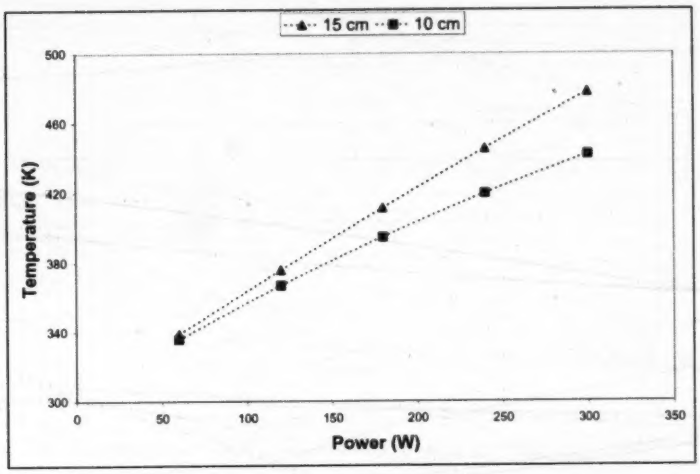

Figure 4.25: **Maximum temperatures plotted as function of power for two target to substrate distances. Data is for aluminum deposition at 10 mTorr.**

As noted in figure 4.25, for low power there is no significant increase in temperature. However, when power is increased, the gas gets hotter in the 15 cm configuration. This could be expected to happen as there is more thermalization of the sputtered particles since more particles deposit their energy into the gas rather than onto the walls.

For concentration profiles, the minimum densities are only slightly reduced when the distance is changed. This could be because, there is more space for rarefaction to occur extending the zone of reduced densities to overcome the effect of the higher temperature. But also remember that density and temperature are inversely proportional, and this difference could be due to this inverse relation.

4.1.5 Cell size effect

Ideally, one would choose a small grid cell to minimize the error introduced in discretizing equations 3.5 and 3.8. However, in reducing the cell size, one loses in performances as more operations are needed due to the increased number of cells. To investigate the effect of reducing the cell's dimensions in the results previously reported, figure 4.27 shows the comparison of two different grid sizes.

As figure 4.27 suggests, the configuration chosen in the present study is sufficient to minimize the discretization error to an acceptable level.

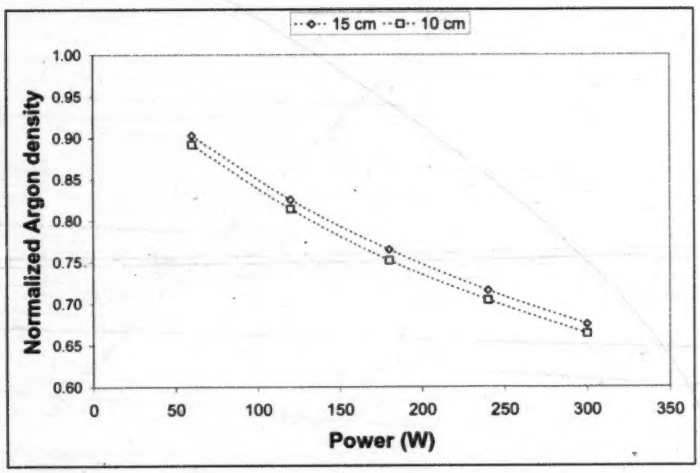

Figure 4.26: **Minimum argon densities as function of power for two target to substrate distances. Data is for aluminum deposition at 10 mTorr.**

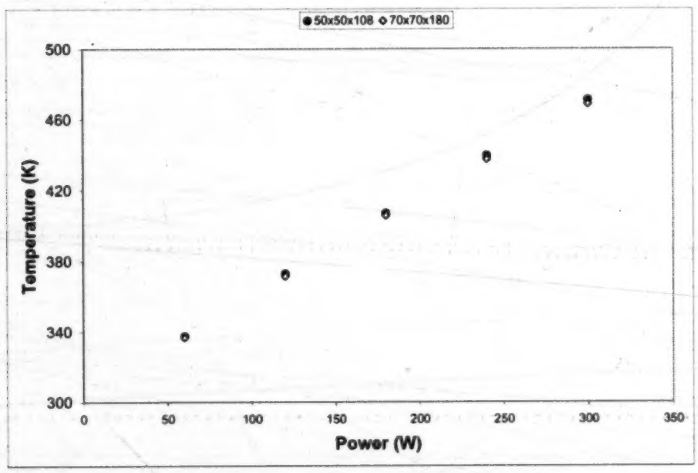

Figure 4.27: **Cell size effect on simulation results for 10 cm target to substrate separation. There is no significant difference when further decreasing the cell size. However, TS1 execution time increased by 13% while TS2 execution increased more than 100%.**

Chapter 5

Conclusions and recommendations

5.1 Conclusions

In this thesis, a sub-module of a suite of simulators for magnetron sputter deposition processes has been presented. This sub-module solves for the transport of thermalized neutral particles plus gas heating and rarefaction in a magnetron sputter deposition system. This is, if not the first, one of the most complete full 3D study to show rarefaction and gas heating in a magnetron system. The module presented is part of a new computational framework capable enough to simulate most configurations used in industry and research. Gas heating and convective mass transport have been incorporated into the model to investigate these effects on gas rarefaction. Quantitative and qualitative agreement with previous works has been found for the gas heating results. Qualitative agreement of gas rarefaction results were observed when compared with other works. A significant neutral depletion effect was found to exist even at low power densities and low pressures. In the following, a brief summary of the principal topics discussed in this thesis is presented.

5.1.1 Gas heating effect

The heating of the background gas has been assumed to be dominated by conduction, and convective heat transfer has been neglected. The main source for the gas heating effect has been assumed to be caused by collisions of energetic sputtered particles ejected from the target. For aluminum deposition, which is the case study presented in this thesis, it was found that the temperature profile follows a predominantly linear behavior with respect to power. However, the effect of pressure on temperature was found to be non linear, at least for the range of pressure investigated here (1-20 mTorr). The location of the maximum temperature shifts toward the cathode as power and pressure increases. Maximum temperature was found also to be sensitive to substrate distance and target material. Coupling between TS1 and TS2 was found to be important as significant differences were found to exist between the results of the first and the last iteration of THERMSPUD. This effect is due to the nonuniform gas density in the high energy module when coupling it with a continuum solver. The change in the final profile is more pronounced for copper than for aluminum due to the higher sputtering yield of copper and the more efficient energy transfer precess of copper in argon.

5.1.2 Rarefaction of background gas

Gas rarefaction was found to be affected by the convective transport of thermalized particles. By omitting this important effect one is underestimating the background density in assuming only diffusive transport. Neglecting momentum transfer from the flux of energetic particles and from fluxes created by pressure gradients was found to be a bad approximation for this problem. Depletion of gas density close to the target was found to be affected the most

by pressure, with reductions as much as 40% of the nominal value at 20 mTorr and 300 W for aluminum. For copper, it was found a 50% reduction for 10 mTorr and 180 W.

5.1.3 Sputtered atoms

Thermalization of sputtered particles was found to be dependent on pressure and power when the target to substrate distance was held constant. It was observed that the diffusive flux of sputtered particles is maximum at about 5 mTorr and it is kept fairly constant above 15 mTorr for a fixed power in the configuration used in this work. This constant flux means that most of the sputtered particles have been thermalized. More thermalization also means a lower energy flux at the substrate.

5.2 Recommendations for future work

The model presented in this thesis can be further improved by including another module to handle the gas and heat interaction at the walls. While the model proposed was designed to minimize this effect, a more detail analysis of it could increase the accuracy of the solver. In adopting such a module one could investigate more complex boundary conditions at the walls (temperature discontinuities at the walls have been sometimes observed in low pressure systems near the walls in near vacuum). Also, the model proposed could be improved by investigating the effect of other models for the scattering cross section and transport coefficients on the final results. However, these improvements are believed to be unlikely to significantly improve the solution as argued before. It could be argued that incorporating convective transport into the energy solver will not affect the equilibrium solution, but this remains to

be seen. Adding gas inlet and outlets into the chamber would be an interesting improvement and it is left for further investigation.

Finally, the integration of all SPUDII modules would greatly help to have a better understanding of the dynamics of the whole sputtering deposition process. At the moment of writing this thesis, some parts of the whole program are not completely linked together and it is not possible to run a full simulation. It is not clear how a full simulation will affect the results reported, hopefully not too much.

Bibliography

[1] S.K. Dew. *Processes and simulation for advanced integrated circuit metallization.* PhD thesis, Electrical and computer engineering, University of Alberta, 1992.

[2] K.L. Chopra and I. Kaur. *Thin film devices applications.* Plenum press, 1983.

[3] D.L. Smith. *Thin film deposition: Principles and practice.* McGraw Hill, 1995.

[4] M. Brett. *Thin film technology.* Course notes, U of A, 1999.

[5] D.M. Mattox. *The foundations of vacuum coating technology.* Noyes publications, 2003.

[6] B.G. Streetman and S Banerjee. *Solid state electronic devices.* Prentice Hall, 2000.

[7] K. Wasa and S. Hayakawa. *Handbook of sputter deposition system.* Noyes Publications, 1992.

[8] S. Leonard. A framework for reactor-scale pvd simulation. Master's thesis, Electrical and Computer Engineering, University of Alberta, 2002.

[9] A. Bogaerts, R. Gijbels, and V.V Serikov. Calculation of gas heating in direct current argon glow discharges. *J. Appl. Phys.*, 87(12):8334, 2000.

[10] G.M. Petrov and C.M. C.M. Ferreira. Numerical modelling of the constriction of the dc positive column in rare gases. *Physical Review E*, 59(3):3571, 1999.

[11] J.D. Bukowski, D.B. Graves, and P. Vitello. Two-dimensional fluid model of an inductively coupled plasma with comparation to experimental spatial profiles. *J. Appl. Phys.*, 80(5):2614, 1996.

[12] E.A. Den Hartog, D.A. Doughty, and J.E. Lawler. Laser optogalvanic and fluorescence studies of the cathode region of a glow discharge. *Physical Review A*, 38(5):2471, 1988.

[13] T. Hory, M.D. Bowden, K. Uchino, K. Muroaka, and M. Maeda. Measurements of electron temperature, electron density, and neutral density in a radio-frequency inductively coupled plasma. *J. Vac. Sci. Technol. A*, 14(1):144, 1996.

[14] K. Muraoka, K. Uchino, and M.D. Bowden. Diagnostics of low-density glow discharges plasmas using thomson scattering. *Plasma Phys. Control. Fusion*, 40:1221, 1998.

[15] S.M. Rossnagel. Gas density reduction effects in magnetrons. *J. Vac. Sci. Technol. A*, 6(1):19, 1988.

[16] T.P. Drusedau. Gas density and throw distance for the sputter deposition of aluminum and tungsten. *J. Vac. Sci. Technol. A*, 20(2):459–466, 2002.

[17] R.E. Somekh. The thermalization of energetic atoms during the sputtering process. *JVT*, 2(3):1285, 1984.

[18] R.E. Somekh. Calculations of thermalization during the sputter deposition process. *Vacuum*, 34(10):987–990, 1984.

[19] A. Bogaerts, M. Van Straaten, and R. Gijbels. Description of the thermalization process of the sputtered atoms in a glow discharge using a three-dimensional monte carlo method. *J. Appl. Phys.*, 77(5):1868, 1995.

[20] K. Meyer, I. K. Schuller, and C. M. Falco. Thermalization of sputtered atoms. *J. Appl. Phys.*, 52(9):5803, 1981.

[21] G.M. Turner, I.S. Falconer, B.W. James, and D.R. McKenzie. Monte carlo calculation of the thermalization of atoms sputtered from a cathode of a sputtering discharge. *J. Appl. Phys.*, 65(9):3671, 1989.

[22] G.M. Turner. Monte carlo calculation of gas rarefaction in a magnetron sputtering discharge. *J. Vac. Sci. Technol. A*, 13(4):2161, 1995.

[23] J.A. Valles-Abarca and A. Gras-Marti. Evolution towards thermalization, and diffusion, of sputtered particle fluxes: Spatial profiles. *J. Appl. Phys.*, 55(5):1370, 1984.

[24] A. Grass-Marti and J.A. Valles-Abarca. Slowing down and thermalization of sputtered particle fluxes: Energy distributions. *J. Appl. Phys.*, 54(2):1071, 1983.

[25] W.D. Westwood. Calculation of deposition rates in diode sputtering systems. *J. Vac. Sci. Technol. A*, 15(1):1, 1978.

[26] Y. Yamamura and M. Ishida. Montecarlo simulation of the thermalization of sputtered atoms and reflected atoms in the magnetron sputtering discharge. *J. Vac. Sci. Technol. A*, 13(1):101, 1995.

[27] T. Motohiro. Applications of monte carlo simulation in the analysis of a sputter-deposition process. *J. Vac. Sci. Technol. A*, 4(2):189, 1986.

[28] C.H. Shon and J.K. Lee. Modeling of magnetron sputtering plasmas. *Applied surface science*, 192:258–269, 2002.

[29] H.M. Urbassek and D. Sibold. Sputtered atom transport in high-current gas discharges: A sele-consistent computer simulation study. *J. Vac. Sci. Technol. A*, 11(3):876, 1993.

[30] J.C. Helmer and C.E. Wickersham. Pressure effect in planar magnetron sputter deposition. *J. Vac. Sci. Technol. A*, 4(3):408, 1986.

[31] A. Bogaerts and R. Gijbels. Role of sputtered cu atoms and ions in a direct current glow discharge: Combined fluid and monte carlo model. *J. Appl. Phys.*, 79(3):1279, 1996.

[32] A. Bogaerts and R. Gijbels. Collisional-radiative model for and argon glow discharge. *J. Appl. Phys.*, 84(1):121, 1998.

[33] V.V. Serikov and K. Nanbu. The analysis of background gas heating in direct current sputtering discharges via particle simulation. *J. Appl. Phys.*, 82(12):5948, 1997.

[34] A.G.L. Borthwick, Marchant R.D., and Copeland G.J.M. Adaptive hierarchical grid model of water-borne pollutant dispersion. *Philos. Mag.*, 18:377, 1968.

[35] A.G.L. Borthwick, Cruz-Leon S., and Jozsa J. Adaptive quadtree model of shallow-flow hydrodynamics. *IAHR J. Hydraulic research*, 39(4):413, 2001.

[36] D. Martin and Cartwright K. Solving poisson's equations using adaptive mesh refinement. Technical Report M96/66, University of Berkeley, Berkeley Electronic Research Laboratory, October 1996.

[37] S. Popinet. Gerris: a tree-based adaptive solver for the incompressible euler equations in complex geometries. *J. Comput. Phys.*, 190:572, 2003.

[38] D. Greaves. A quadtree adaptive method for simulating fluid flows with moving interfaces. *J. Comput. Physis.*, 194(1):35–56, 2004.

[39] B. Chapman. *Glow discharge processes.* Wiley publications, 1980.

[40] M.W. Thompson. Energy deposition. *Philos. Mag.*, 18:377, 1968.

[41] R.S. Robinson. Energetic binary collisions in rare gas plasmas. *J. Vac. Sci. Technol.*, 16:185, 1979.

[42] A.V. Phelps. The application of scattering cross-sections to ion flux models in discharge sheats. *J. Appl. Phys.*, 76(2):747, 1994.

[43] A. Kersch, W. Murokoff, and C. Werner. Selfconsistent simulation of sputter deposition with monte carlo method. *J. Appl. Phys.*, 75(4):2278, 1994.

[44] D.W. Hoffman. A sputtering wind. *J. Vac. Sci. Technol. A*, 3(3):561, 1985.

[45] H.K. Versteeg and Malalasekera W. *An introduction to Commputational Fliud Dynamics: the finite volume method.* Prentice Hall, 1995.

[46] C. Kittel and H. Kroemer. *Thermal Physics.* W.H. Freeman and Company, 1980.

[47] E.L. Cussler. *Diffusion, mass transfer in fluid systems.* Cambridge University Press, 1984.

[48] J.C. Tannehill, D.A. Anderson, and Pletcher R.H. *Computational fluid mechanics and heat transfer.* Taylor and Francis, 1997.

[49] E.H. Kennard. *Kinetic theory of gases.* McGraw Hill, 1934.

[50] A.V. Phelps, C.H. Green, and J.P. Burke. Collision cross sections for argon atoms with argon atoms for energies from 0.01 ev to 10 kev. *J. Phys. B: At. Mol. Opt. Phys.*, 33:2965, 2000.

[51] V.V. Serikov and K. Nanbu. Monte carlo numerical simulation of target erosion and film growth in a three-dimensional sputtering chamber. *J. Vac. Sci. Technol. A*, 14(6):3108, 1996.

[52] T.P. Redko, Rusinov I.M., and Blagoev A.B. Diffusion of ground state($3s^2\,{}^1s_0$) and metastable($3s3p\,{}^3p_{0,1,2}$) magnesium atoms in he and ne. *J. Phys. B: At. Mol. Opt. Phys.*, 26:107–111, 1993.

[53] S.V. Patankar. *Numerical heat transfer and fluid flow.* McGraw-Hill, 1980.

[54] H.Z. Barakat and J.A. Clark. Analytical and transient study of transient laminar natural convection flows in partially filled containers. *Proc. 3rd. Int. Heat Transfer Conf.*, 2:152, 1966.

[55] D.L. Scharfetter and H.K. Gummel. Large-signal analysis of a silicon read diode oscillator. *IEEE Trans. Elect. Dev.*, 16(1):64, 1969.

[56] J.D.P. Pashier and W.J. Goedheer. A two-dimensional fluid model for an argon rf discharge. *J. Appl. Phys.*, 74(6):3744, 1993.

[57] J.D.P. Pashier and W.J. Goedheer. Relaxation fenomena after laser-induced photodetachemnte in electronegative rf discharges. *J. Appl. Phys.*, 72(3):1073, 1993.

[58] A. Bogaerts, R. Gijbels, and W.J. Goedheer. Hybrid monte carlo-fluid model of a direct current glow discharge. *J. Appl. Phys.*, 78(4):2233, 1995.

[59] J.P. Boeuf. A two-dimensional model of dc glow discharges. *J. Appl. Phys.*, 63:1342, 1988.

[60] S. Selberherr. *Analysis and simulation of semiconductor devices.* Springer-Verlag Wien-New York, 1984.

[61] D.B. Spalding. A novel finite difference formulation for differential expressions involving both first and second derivatives. *Inter. J. Num. Meth. Eng.*, 4(2):551, 1972.

[62] G.D. Raithby and K.E. Torrance. Upstream-weighted differencing schemes and their application to elliptic problems involving fluid flow. *Computers and fluids*, 2:191, 1974.

[63] A.K. Runchal. Convergence and accuracy of three finite difference schemes for a two-dimensional conduction and convection problem. *Inter. J. Num. Meth. Eng.*, 4(2):541, 1972.

[64] E.F. Nogotov. *Applications of numerical heat transfer.* Mc Graw-Hill, 1978.

[65] G. De Marsily. *Quantitative hydrogeology: Groundwater hydrology for engineers.* Academic press, 1986.

[66] R.W. Hockney and J.W. Eastwood. *Computer simulation using partilcles.* Prentice Hall, 1980.

[67] M.J. Holst and F Saied. Numerical solution of the nonlinear poisson-boltzmann equation: Developing more robust and efficient methods. *J. Comput. Chem.*, 16:337, 1995.

[68] M. Stepanova and S.K. Dew. Discrete-path transport theory of physical sputtering. *J. Appl. Phys.*, 92(3):1699–1708, 2002.

[69] S. Liu. A target module in a sputter deposition simulation system. Technical report, University of Alberta, This films, November 2003.

[70] J.R. Tynan. Neutral depletion and transport mechanisms in large-area high density plasma sources. *J. Appl. Phys.*, 86(10):5356–5364, 1999.

[71] M.D. Kilgore, Wu H.M., and Greaves D.B. Neutral trasnport in high plasma-density reactors. *J. Vac. Sci. Technol. B*, 12(1):494–506, 1994.